FE-2229-5
Distribution Category UC-90c

SURFACE STRUCTURE AND MECHANISMS OF GASIFICATION CATALYST DEACTIVATION

Quarterly Report for the Period
January – April 1977

P. J. Reucroft
E. B. Bradley
R. J. De Angelis
G. A. Sargent

Date Published
August 1977

Under Contract No. EX-76-C-01-2229
(formerly E(49-18)-2229)

PREPARED FOR
ENERGY RESEARCH AND DEVELOPMENT ADMINISTRATION

UNIVERSITY OF KENTUCKY
Lexington, Kentucky 40506

355 4010

ACKNOWLEDGMENTS

Catalyst samples and general information were supplied by A. L. Hausberger and Associates at Catalysts and Chemicals, Inc., Louisville, Kentucky.

I. ABSTRACT

Additional ESCA standard samples (NiS, $NI(OH)_2$) have been examined, NiS was found to have very little surface charging and small chemical shifts (compared to the Ni metal). A quantitative analysis of the L140 catalysts revealed that the particle sizes do not change greatly with increasing metal loading. The binding energies and peak shapes correspond to a nickel aluminate complex. Two used catalysts were studied in order to assess the effects of exposure to synthesis gas and presulfiding. The presulfiding treatment effectively saturated the catalyst with sulfur.

Thermal gravimetric analysis has been used to study the reduction kinetics of NiO dispersed on silica and alumina supports. Data showing effects of temperature and hydrogen flow rates on the reduction kinetics of these catalysts are presented and discussed.

Raman spectra have been obtained of the SiO_2 and Al_2O_3 support materials which show very weak bands characteristic of amorphous solids. Photodecomposition of $NiCO_3$ and $NiSiO_3$ samples limited incident laser power but their Raman band intensities are also small. Fluorescence did not obscure the Raman bands of these powdered samples but is shown to depend on sample preparation and handling. The Raman spectrum was also obtained of the sulphided alumina-support catalyst which shows characterisitc sulphate and sulphite bands.

Auger electron spectroscopy was employed for the study of the elemental depth distribution of the Ni catalysts. The result has shown that a contaminated layer of depth 400Å was present on the surface. NiO particles were more susceptible to the contamination than Al_2O_3 particles. The Auger electron escape depth for SiO_2 supported catalysts is about the same as for Al_2O_3 supported catalysts.

II. OBJECTIVE AND SCOPE OF WORK

The objective of the program is to characterize the surface structure of methanation catalysts in order to relate structural features to catalytic activity and catalyst deactivation. Surfaces to be examined include (a) single crystal nickel with well-defined crystal planes and (b) dispersed samples of nickel and nickel alloys on alumina and silica supports. The chemical composition and surface concentration will be measured by ESCA and Auger Spectroscopy. Chemical bonding information will be determined by Raman and infrared spectroscopy. Structural changes in the surface lattice will be investigated by LEED characterization. The catalyst surface will be investigated in the presence of CO, H_2, CH_4 and H_2S in the initial stages of the program. Other potential poisons and deactivating agents, such as chlorides, cyanides, nitrogen oxides and carbon depositors such as ethylene and benzene will be investigated as the program develops. The validity of currently accepted models of catalyst thermal deactivation i.e. sintering, will be evaluated and assessed for accuracy and applicability. Parameters to be monitored include (a) particle size and particle size distribution, (b) the effect of temperature on particle size distribution, and (c) the effect of particle size distribution on the rate of thermal sintering.

III. SUMMARY OF PROGRESS TO DATE

After extensively investigating coprecipitated nickel methanation catalysts (metal loading, 10-50% by weight) by the ESCA techniques, studies are now being directed toward catalysts that have been employed in methanation reactors. Active catalysts with good methanation activity and sulfur deactivated catalysts have been examined.

X-ray diffraction techniques for determining catalyst particle size distributions have been improved and refined in a series of studies on nickel oxide dispersed in alumina and silica. Studies are now focussed on determining the effect of time and temperature on the particle size distribution in reduced coprecipitated catalysts, in order to gain insight into the thermal sintering mechanism.

The studies on chemical bonding in several alumina and silica supported coprecipitated nickel methanation catalysts have emphasized infrared spectroscopy in the initial stages of the program. Fresh catalysts, poisoned (deactivated) catalysts and catalysts that have been employed in methanation reactors, have been examined. These materials are currently being investigated by laser Raman spectroscopic techniques. Adsorbed gas monolayers on single crystal surfaces will be investigated by laser Raman and infrared spectroscopy in the next phase of the program.

Auger spectroscopy has been employed to investigate atom distributions in catalyst pellets. Both fresh and used catalysts have been employed in these studies. Single crystal specimens, suitable for LEED studies on both clean surfaces and adsorbed monolayers, are currently being prepared. A more detailed description of the research activities in the past quarterly period is presented in subsequent sections.

The status of the project to date is illustrated in Figure III. 1. Task areas 1 and 4 are approximately on schedule. Task areas 2 and 3 are judged to be approximately three months behind schedule, due to delays in receiving equipment and the delayed appointment of research personnel in these areas. The project costs are approximately at the budgeted level.

Several manuscripts describing the more significant results obtained on the project to date are currently in preparation and will be submitted to journals in the near future. The following presentations will be delivered at scientific and engineering meetings in the next quarter:

1. "Characterization of Heterogeneous Catalysts," to be presented by R. B. Shalvoy at the Northeast ESCA Users Group Meeting XII, Wilmington, Delaware, May 20, 1977. In addition Dr. Shalvoy will act as discussion leader for the session, "Industrial Catalysts and Inorganic Complexes."

2. "ESCA Characterization of Methanation Catalysts," by P. J. Reucroft, B. H. Davis and R. B. Shalvoy, to be presented by P. J. Reucroft at the Symposium on Catalysis of Coal Conversion Processes, Second Joint Chemical Institute of Canada - American Chemical Society Conference, Montreal, May 29-June 2, 1977.

3. "Particle Size Distribution Functions of Supported Metal Catalysts by X-ray Diffraction," by R. J. De Angelis, P. Ganesan and A. Saavedra, to be presented by R. J. De Angelis at the Symposium on Catalysis of Coal Conversion Processes, Second Joint Chemical Institute of Canada - American Chemical Society Conference, Montreal, May 29 - June 2, 1977.

4. "Infrared and Raman Spectra of a Heterogeneous Nickel-Alumina Catalyst," by J. M. Stencel and E. B. Bradley, to be presented by J. M. Stencel at the 32nd Symposium on Molecular Spectroscopy, Ohio State University, Columbus, Ohio, June 13 - 17, 1977.

Research personnel who are currently participating in the project, in addition to the co-principal investigators, include Drs. P. Ganesan, R. B. Shalvoy, J. M. Stencel and C. H. Huang (Postdoctoral Research Associates) and several graduate assistants.

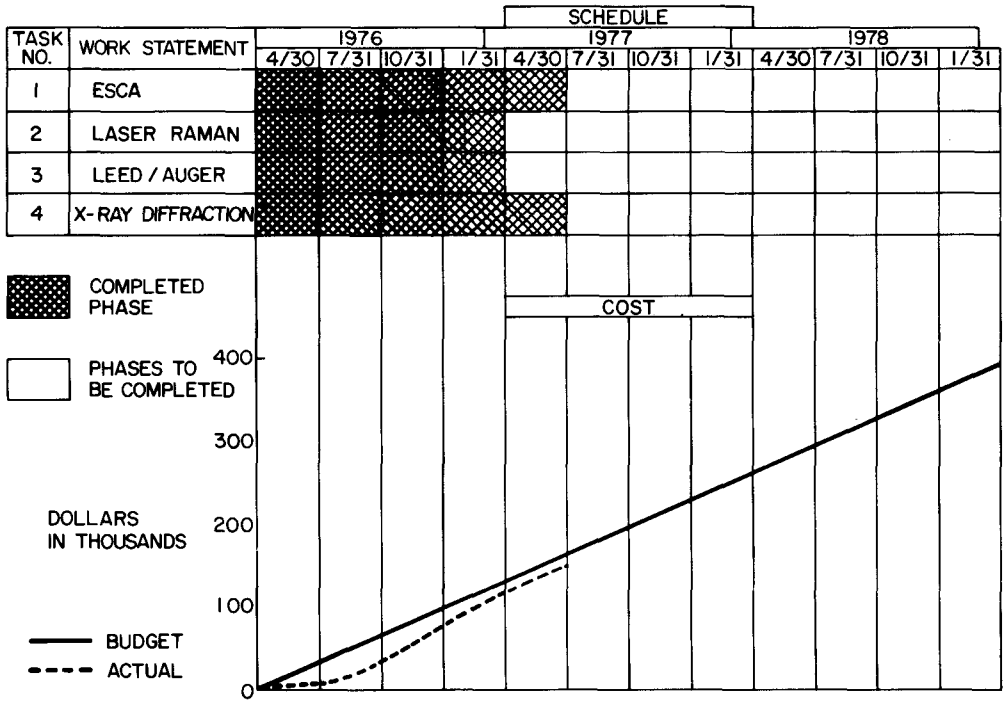

Figure III 1. Summary of Project Progress.

IV. DETAILED DESCRIPTION OF TECHNICAL PROGRESS

A. REPORTING CATEGORY 1 - ESCA STUDIES (Prepared by R. B. Shalvoy and P. J. Reucroft)

(i) Work Accomplished

Work in the past quarter has proceeded in several directions. Some instrumental problems have been encountered, but the initial phases of the project are nearing completion with papers being prepared for publication.

Instrumental Modifications

The parts for a charge neutralizing flood gun[1] have been assembled. Some problems in preparing the filament have been encountered. These have now been overcome and we expect to test the flood gun in the next quarter.

A manifold for admitting pure gases into the spectrometer in precisely controlled amounts has been designed and the necessary parts are on order or have already been delivered. The design of the manifold is shown in Figure IV A1. This design allows admission of research grade gases independently or in conjunction with other gases. The gases may be changed easily without venting the manifold. One admission line has been constructed of stainless steel parts for use with corrosive gases such as H_2S or SO_2.

Standard Samples

A few additional standard samples have been examined. $Ni(OH)_2$ may be present in some nickel oxide samples[2] or used catalysts.[1] NiS is a compound which may occur in poisoned catalysts (Ni_2S or Ni_4S have also been suggested as surface forms for sulfur on Ni(100)[3]). A $NiSO_4$ sample has been ordered.

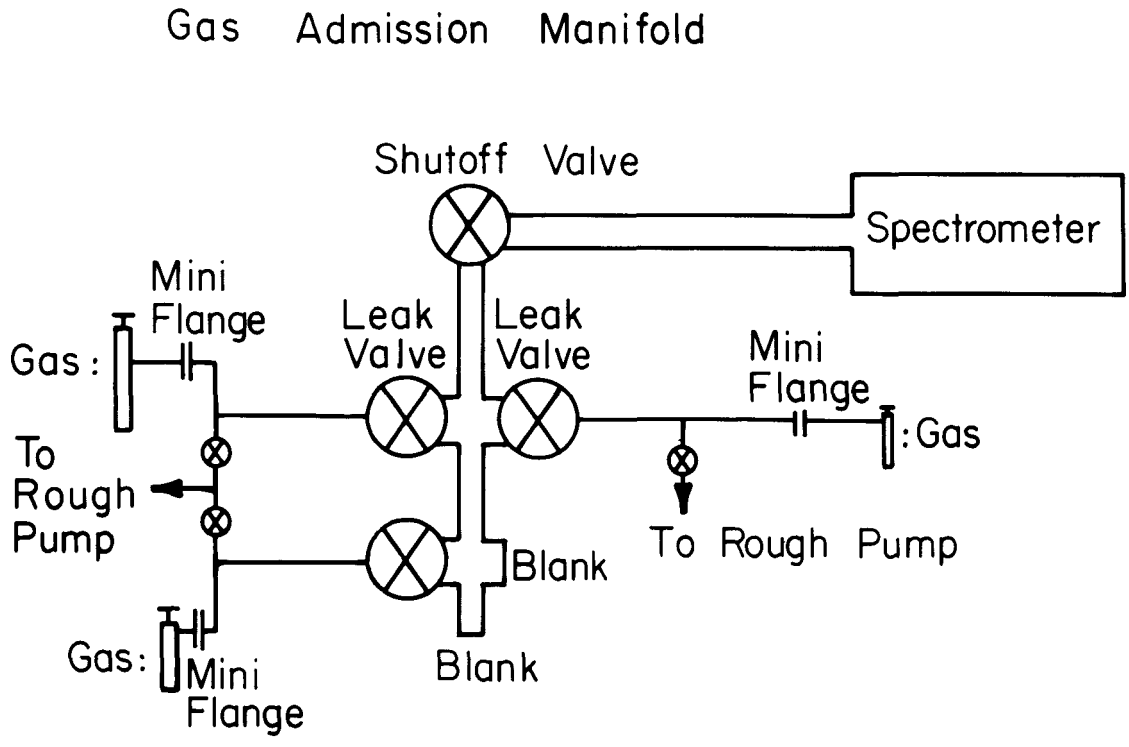

Figure IV A1. Schematic diagram of the Gas Admission Manifold. Thick lines represent high vacuum area, thin lines represent low vacuum regions.

$Ni(OH)_2$ is of interest as a compound possibly occurring in the catalyst samples. It has been reported that $Ni(OH)_2$ undergoes a partial reduction to NiO and Ni under heating at 250°C in situ.[4] Argon ion etching (600eV, 3 min.) did not further reduce the sample. The results shown in Figure IV A2 are generally in agreement with these findings. It was observed, however, that more severe etching (1500eV, 30 min.) caused some reduction of the sample. This result is to be expected as the free energy of formation of the hydroxide is low enough so that the higher electron beam energy employed is sufficient to cause some reduction.

$Ni(OH)_2$ charges to an appreciable extent (2 eV). The main Ni $2p_{3/2}$ peak does not show the doublet structure observed for NiO. The O $1s_{1/2}$ peak is also a singlet. Extended argon ion etching radically alters the spectrum. Examination of the etched spectrum indicates that the sample is a mixture of NiO, Ni and $Ni(OH)_2$, as shown in Figure IV A2.

The NiS sample was obtained from Alfa Inorganics as a black, somewhat gritty material. The spectra (Figure IV A3) are somewhat different from those obtained for other standard samples as there is practically no charging of the surface and the chemical shifts of the binding energies are quite small.[5] The prominent Ni 2p charge transfer satellite structure is not seen in this material. The valence band shown in Figure IV A4 has a strong peak at 1.6 ev binding energy due to the Ni 3d orbitals and a second peak at 4.2 eV due to the sulfur 3p orbitals. The rise at 14 eV is due to either a plasmon loss mechanism or to the S 3s orbitals.

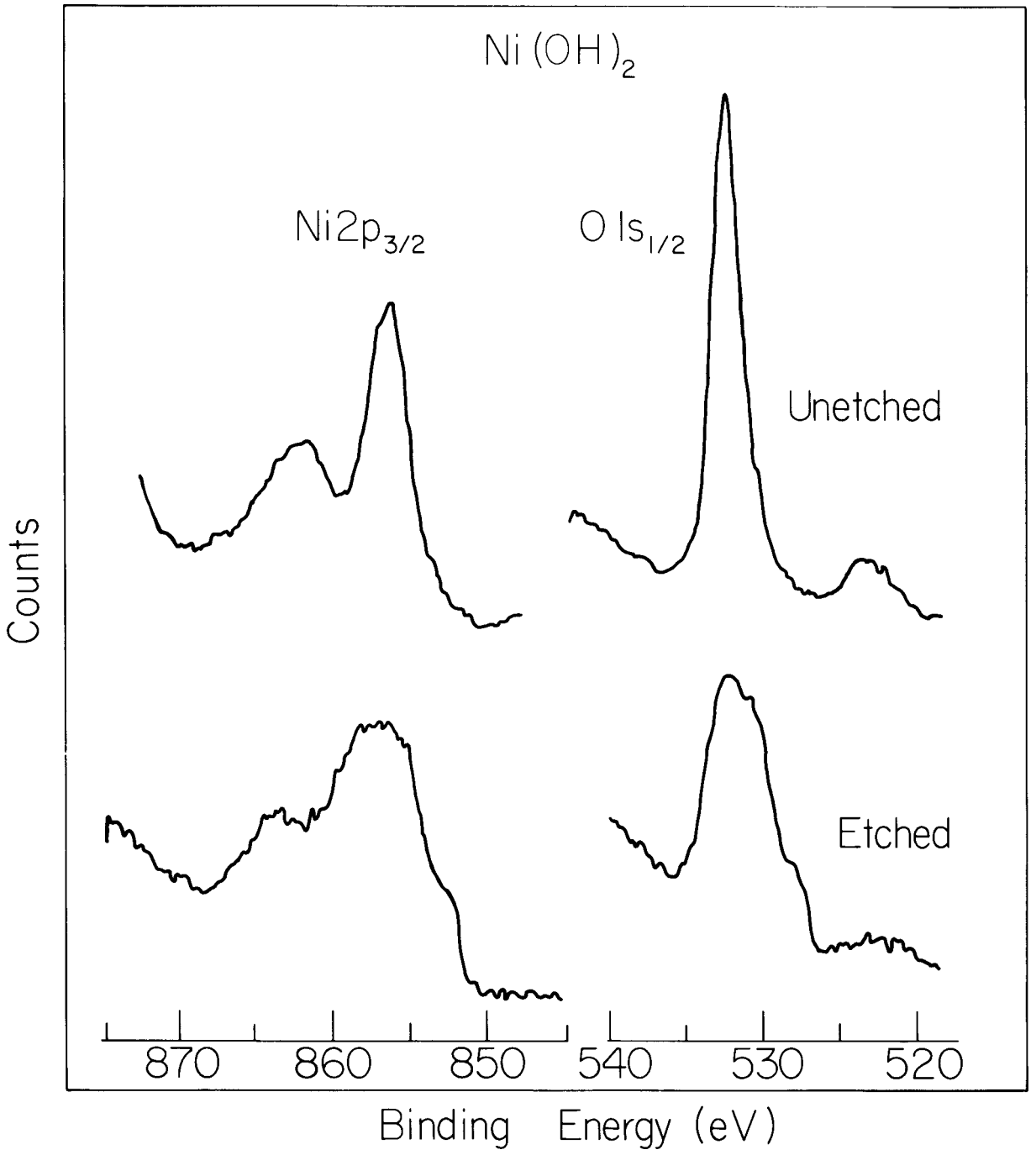

Figure IV A2. ESCA Spectra (Ni $2p_{3/2}$, O $1s_{1/2}$) of $Ni(OH)_2$ as received and after severe etching.

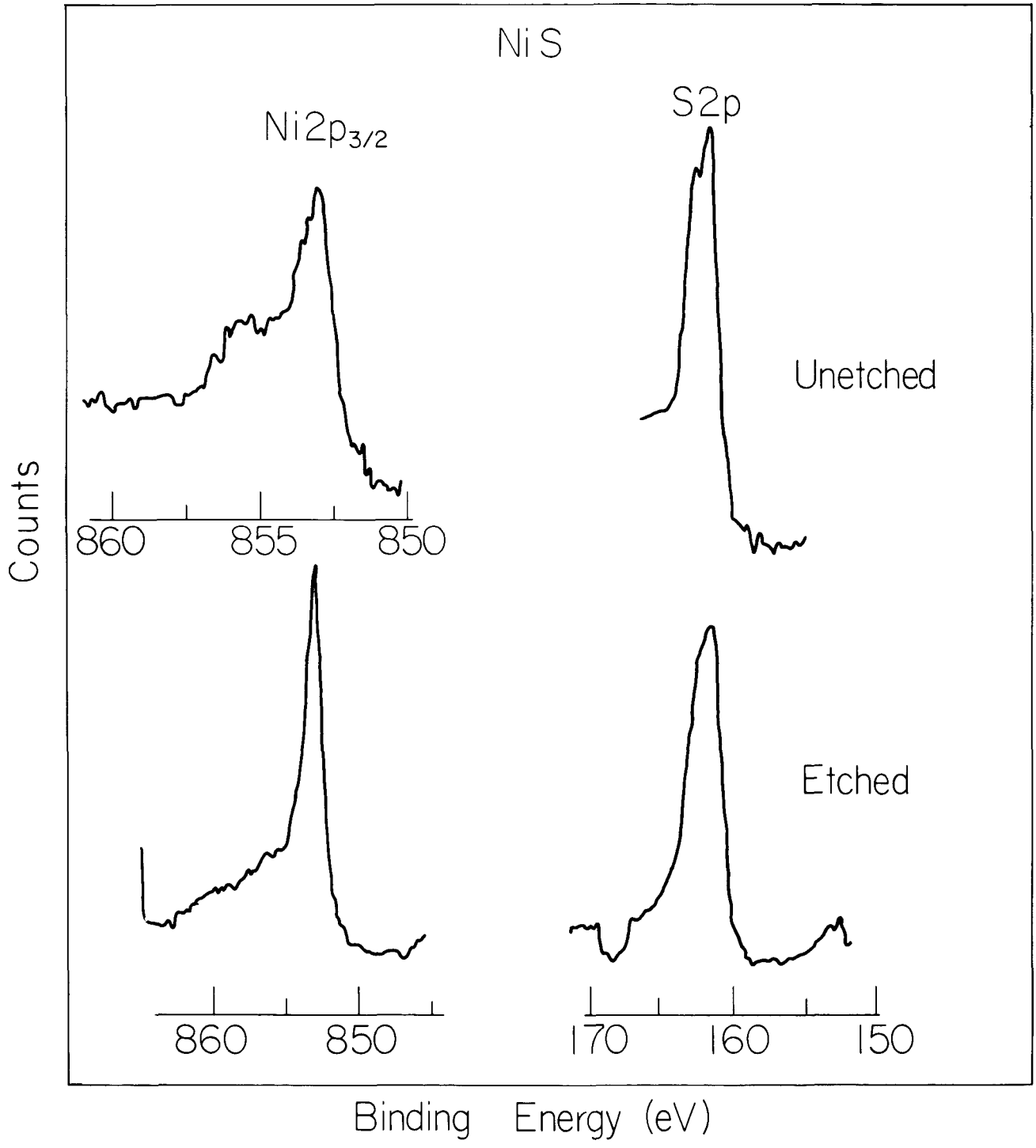

Figure IV.A3. ESCA Spectra (Ni $2p_{3/2}$, S2p) of NiS.

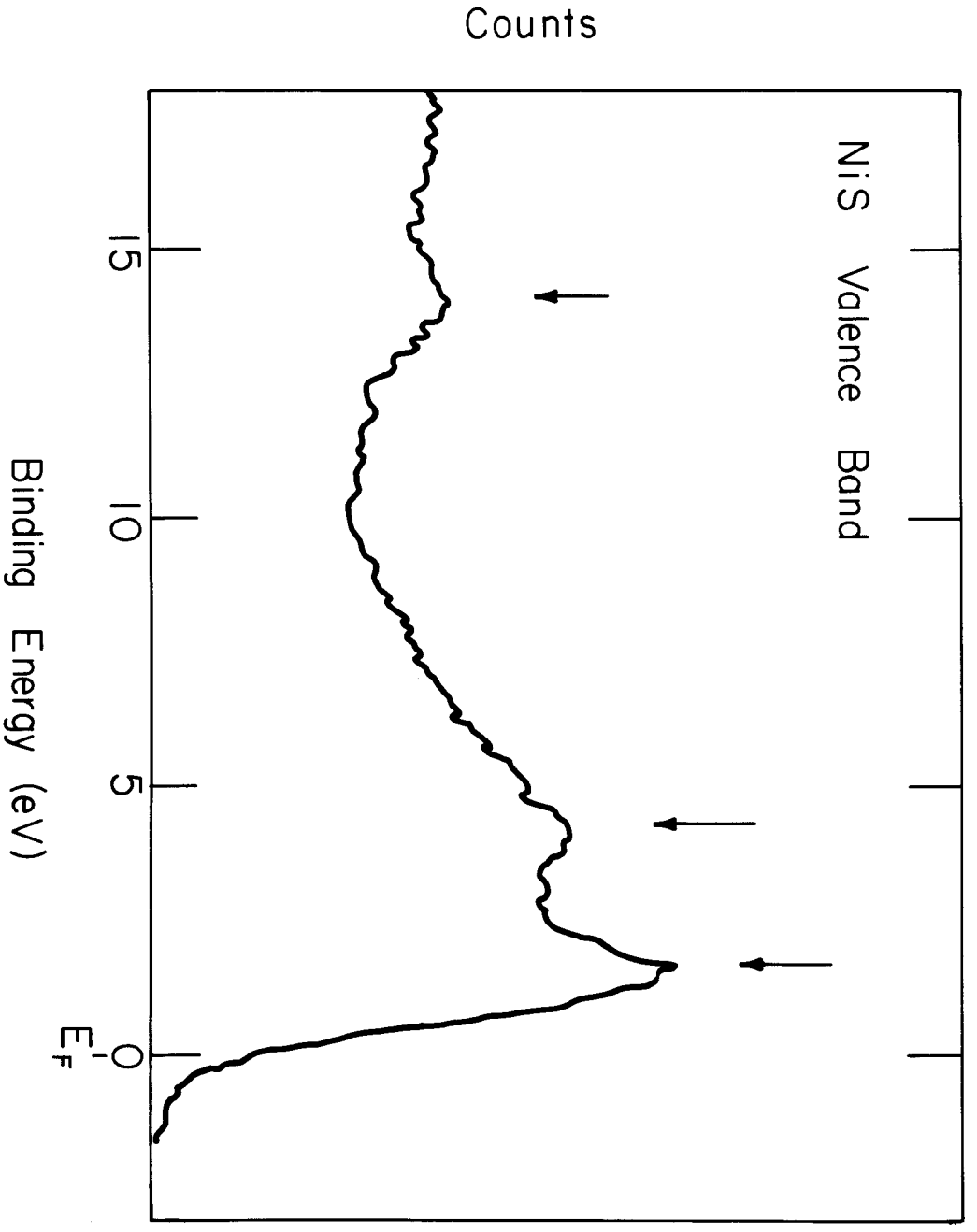

Figure IV A4. Valence band region of NiS. The Fermi level (zero of binding energy) is indicated.

This material is easily distinguished from the other Ni compounds studied, but it is difficult to clearly resolve the Ni 2p peak for NiS from that due to Ni metal. The position of the S peaks should allow indentification of the presence of this compound. The charge corrected binding energies for NiS and $Ni(OH)_2$ are listed in Table 1.

Identification of the presence of NiO in the presence of other Ni compounds has been considered previously.[1] It is uncertain whether the doublet structure of the Ni 2p peak is characteristic of NiO or whether in appropriate forms the peak can occur as a singlet. A series of $(NiO)_x(MgO)_{1-x}$ samples have been shown to have a singlet Ni 2p peak structure.[6] This suggests that the occurence of the doublet is due in part to the interactions of nickel atoms with neighbors and next nearest neighbors.[6] The mechanism responsible for the doublet structure is unresolved. Several possibilities were discussed previously.[1] No explanation is entirely satisfactory. This question will be considered as time permits from the viewpoint of catalyst characterization, it is expected that NiO will have a doublet structured peak in most of its forms.

L140 Catalysts Series

(i) Quantitative Analysis of Signal Intensities

Preliminary studies of the L140 catalyst series (10-40% nickel by weight) have been continued on unreduced samples. ESCA studies have been reported previously on catalysts prepared by impregnation and cation exchange.[7-9] Good correlations were reported between the signal intensities and certain familiar catalyst properties, such as dispersion and particle sizes. It was observed that the shape of the curve for the signal intensity ratio R(Ni 2p/Al 2s) versus the metal loading depends on the method of preparation and may be related to changes in the particle sizes.

The L140 catalyst series differs from these previously investigated catalysts in that they were prepared by coprecipitation with generally higher metal contents. This method of preparation has yielded very active catalysts following reduction of the nickel oxide to nickel metal.[10,11] Particle sizes in the unreduced catalysts, determined by x-ray diffraction, range from 15-30Å,[1] although the particle sizes for the 10-30% nickel samples have not been determined to date.

The intensity of a photoelectron peak for a sample of uniform composition may be described in terms of the following:[12]

$$I = I_0 n \sigma \lambda(\varepsilon)\, D(\varepsilon) \qquad (1)$$

Where I_0 is the x-ray flux, n the density of atoms, σ the photoexcitation cross section, $\lambda(\varepsilon)$ the mean free path of the electron of energy ε in the sample material, and $D(\varepsilon)$ is the detector efficiency. We assume I_0 to be constant and the variations of the mean free path between different catalyst samples to be small. The ratio of intensities of the Ni $2p_{3/2}$ and Al $2s_{1/2}$ core levels, abbreviated to Ni and Al, may be expressed as:

$$R\left(\frac{Ni}{Al}\right) = \frac{I_{Ni}}{I_{Al}} = \frac{n_{Ni}}{n_{Al}} \left(\frac{\sigma_{Ni}\lambda(\varepsilon_{Ni})D(\varepsilon_{Ni})}{\sigma_{Al}\lambda(\varepsilon_{Al})D(\varepsilon_{Al})}\right) = \frac{n_{Ni}}{n_{Al}} (Y) \qquad (2)$$

The term relating the relative atomic density to the ratio of ESCA signal intensities (Y) may be determined from standard samples of known composition. Thus by measuring the relative ESCA signal intensities for the Ni $2p_{3/2}$ and Al $2s_{1/2}$ core levels, the relative atomic abundances of nickel and aluminum in the surface region of the catalyst may be estimated.

The samples were examined in pellet form as received. Surfaces were briefly argon ion etched (1 min., 1 keV beam energy) before examination. It was observed that etching for 30 minutes did not alter the Ni/Al signal ratio appreciably. The known composition samples (NiO and Al_2O_3) and the catalysts were all studied as a consecutive series to minimize the effects of any instrumental changes. The ESCA spectra shown in Figure IV A5 are typical of the results

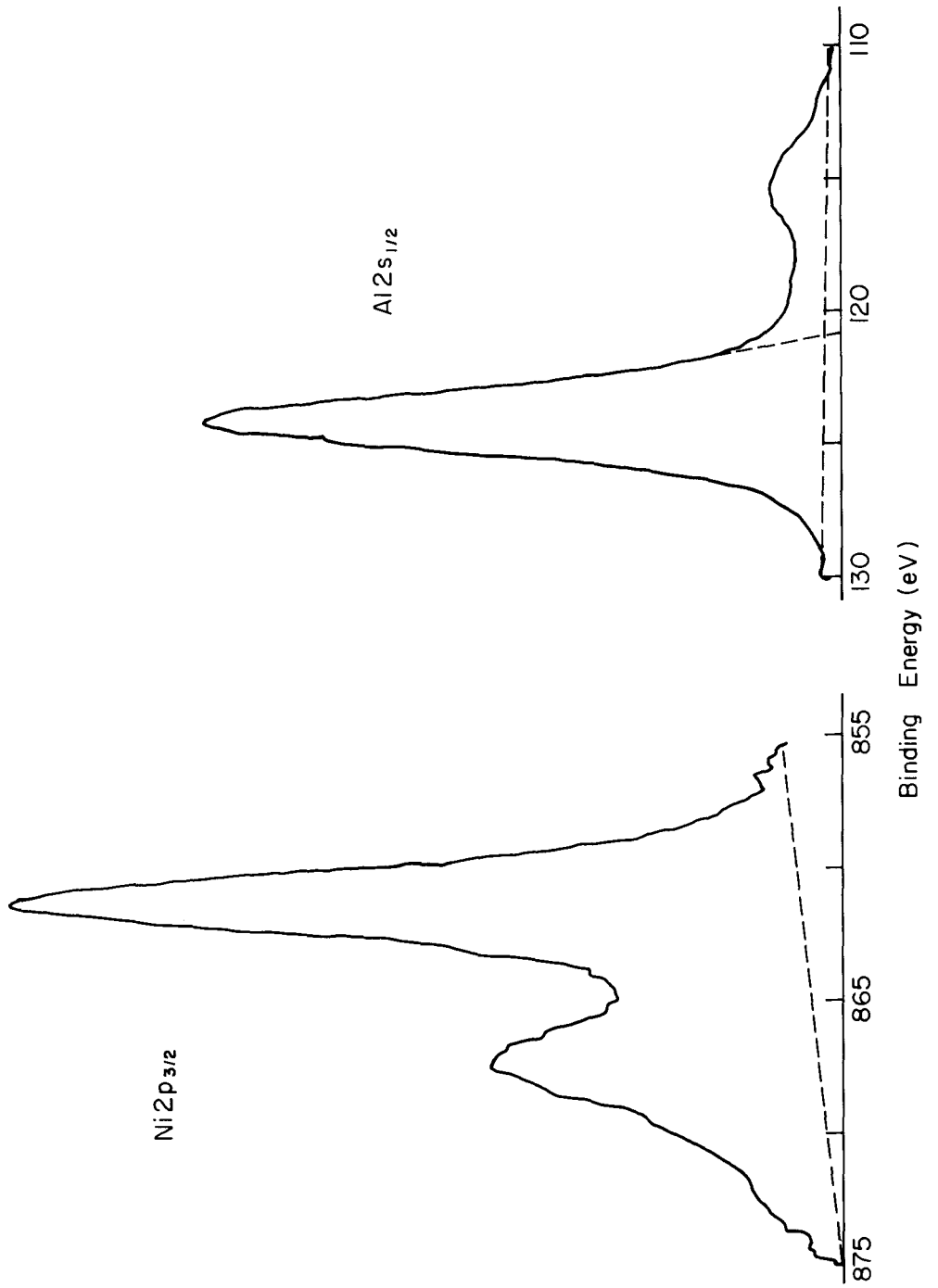

Figure IV A5. Typical ESCA Peak areas measured (L141 sample).

obtained on the catalysts investigated. The peak areas were measured over the areas shown in Figure IV A5. The area of the Al 2s peak was truncated on the low binding energy side as the Ni 3s peak occurs just below the Al 2s peak. The Ni 3s peak is not distinctly visible in this Figure because the nickel content is low. The peak was discernible, however, in the samples of greater nickel content.

The anticipated intensity ratio for these samples was calculated by assuming a sample composition of $(NiO)_x(Al_2O_3)_{1-x}$ and determining the atomic abundances as a function of the specified nickel weight contents. The ESCA peak area ratios were then estimated using equation 2. The atomic abundances, calculated ESCA signal ratios and the experimentally determined peak area ratios are listed in Table 2. The experimentally determined peak area ratios and the calculated ratios are plotted in Figure IV A6 as a function of increasing nickel content.

The agreement between the experimental data and the calculated curve is quite good except for the 47% nickel content sample. Within the experimental uncertainties there is no appreciable difference between theory and experiment in the case of the lower nickel content samples. This result supports the assumptions concerning the sample uniformity and variation of the mean free path between catalyst samples. The result also suggests that the particle size of the unreduced nickel oxide remains relatively constant over the range of nickel contents studied. Particle sizes observed independently for these materials are about equal to the mean free path for the photoelectrons (~15A).[1,13]

The deviation of the higher nickel content sample from the calculated curve may be due to this sample having been reduced prior to the study and thereby possessing a larger particle size. This effect has been noted for other lower metal content samples.[9] This possibility will be tested by examining reduced

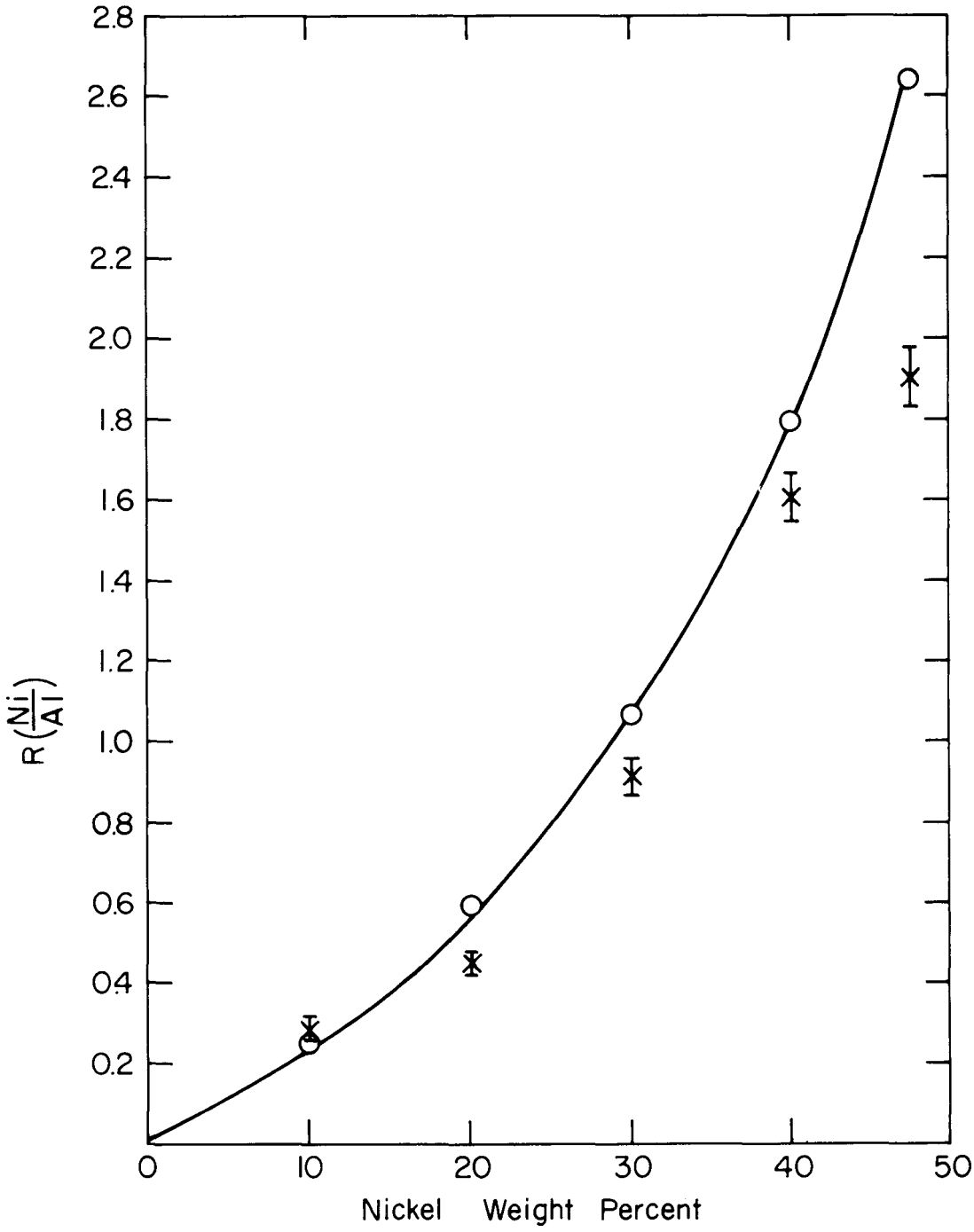

Figure IV A6. Comparison of the experimental and calculated $R(\frac{Ni}{Al})$ intensity ratios for the L140 catalyst series.

and/or sintered forms of the lower nickel content samples and determining their particle sizes independently. It may be possible in this way to determine particle sizes of dispersed metals from ESCA signal intensities while the sample is maintained under vacuum, or for samples which are difficult to evaluate in conventional fashion.

In Figure IV A6, the relationship between the signal intensity ratio and the nickel content corresponds more closely to that observed for low metal content catalysts prepared by a cation exchange method rather than the relationship observed for impregnated catalysts.[9] The catalysts prepared by the cation exchange method were considered to have smaller particle sizes for a given metal loading and this resulted in a curve similar to that observed for the coprecipitated catalysts. The high catalytic activity observed for catalysts prepared by the coprecipitation method may be thus related to the small particle size, evidenced even for the high nickel content samples by the shape of the observed curve as well as by the generally good agreement between the experimental and calculated signal intensity ratios.

A quantitative analysis of ESCA spectra of the dispersed catalyst metal and the support material suggest that the coprecipitation method of preparation provides a good dispersion of the metal even for high metal contents. The reduction process which causes a degree of sintering is reflected in a lower Ni/Al signal intensity ratio. Hence ESCA provides a convenient method of monitoring catalysts' particle sizes, even under vacuum conditions. The analysis on which these conclusions are based is still quite approximate. The reasonable results obtained at this level of analysis is encouraging, however, and indicates that further refinement in the method will lead to the development of a useful catalyst characterization technique.

(ii) Core Level Binding Energies and Surface Characterization

The binding energies of the Ni 2p, O 1s, and the Al 2s core levels have been determined for the unreduced catalyst samples. Charging of about 4 eV has been observed. The binding energies have been corrected for charging using the observed binding energy of the C 1s level from the graphite present in the sample. A value of 285.0 eV is used conventionally for the uncharged position of this level. This method of correction is compatible with the silver dot technique used alternatively.

The corrected binding energies are listed in Table 3. There is a general agreement of the binding energies for all four samples. The shape of the peaks is singlet in nature (Figure IV A7), both before and after extended etching (30 min.). This shows the uniformity and stability of the compounds. The peak shapes are quite consistent for all samples. The spectra are simple, in constrast to the structure observed for the NiO samples. The spectra could be attributed to Ni_2O_3 [4] but the agreement of the binding energies is not very good and Ni_2O_3 has been reported to be thermally unstable and probably could not have survived the extended etching.[4] It can be concluded, therefore, that the samples are primarily a nickel-alumina complex form. As we have not measured the exact binding energies of nickel aluminate this conclusion is tentative, but appears to be reasonable. It is expected that new samples of nickel aluminate and nickel silicate will be prepared early in the next quarter to further clarify these conclusions.

Used Catalysts

The study of used catalysts is one of the more promising areas for the application of ESCA to the catalyst characterization problem.[14] Qualitative, quantitative analyses, and charge state information are all useful in understanding

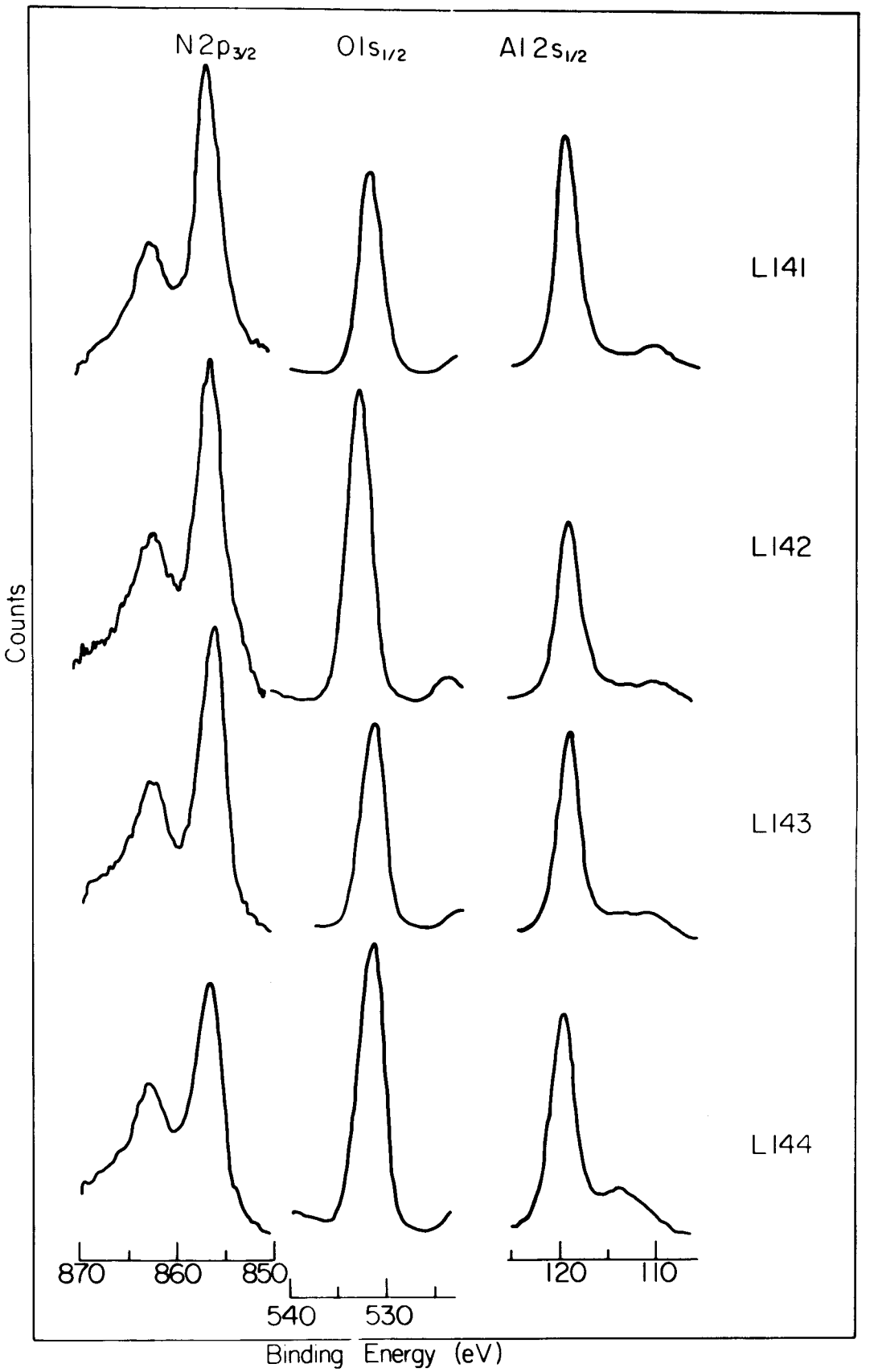

Figure IV A7. ESCA Spectra (Ni $2p_{3/2}$, O $1s_{1/2}$, Al $2s_{1/2}$) of the L140 catalysts. Little difference was observed between the unetched and etched spectra.

the changes undergone by the catalyst while in use. We have made preliminary studies of two catalysts treated by Catalysts and Chemicals, Inc. Infrared studies on these two samples have been reported previously.[1] On the basis of the data accumulated thus far, we are attempting to understand the effects of the various treatments on the catalyst surface.

(i) Run 77, C-150-1-01

This sample was reduced, exposed to synthesis gas and was observed to have very good methanation activity. The sample was examined in the ESCA spectrometer in as received and etched conditions, the sample temperature being 40°C for all runs.

The binding energies corrected for charging are listed in Table 4. The spectra of the Ni 2p, O 1s, and Si 2p core levels are shown in Figure IV A8 for the unetched and progressively etched sample. The binding energy positions of NiO, Ni_2O_3, nickel silicate complex, and $Ni(OH)_2$ are also indicated. The experimental findings for the unetched sample are strongly reminiscent of the nickel silicate complex or $Ni(OH)_2$ standard samples both in binding energies and peak shapes. NiO is definitely not present. A wider scan of the spectrum revealed no unexpected elements. This is in agreement with the infrared results.[1]

Moderate etching reveals a different spectrum. A peak corresponding to nickel metal is now prominent, although the nickel silicate complex/$Ni(OH)_2$ signal is still present in significant amounts in the etched sample spectrum. The oxygen spectrum is unchanged, in agreement with the interpretation of the new peak being due to nickel metal.

Following etch 2, the ratio of Ni^{+2} to nickel metal decreases with a new peak, indicated by an asterisk, appearing in both the nickel and oxygen spectra.

These peaks are due to nickel metal and oxygen peaks that are not shifted by the charging of the sample surface. As a consequence they are shown in a false position in Figure IV A8. They should line up with the charge corrected nickel metal and oxygen peaks. The Si peak also shows evidence of this effect. Etch 3 continues to develop this trend, but we observe that even after extended etching, an appreciable amount of nickel remains in chemically combined form. This result is in agreement with the results obtained on fresh catalyst samples studied previously.[1]

It can be concluded that the test running of this sample has led to the formation of a Ni-SiO_2-OH complex. A significant amount of the nickel is present as nickel metal, particularly in the bulk of the sample. All elements observed were also observed in the freshly reduced/untested catalysts. The occurence of the hydrated complex is not unexpected given the appreciable steam in the synthesis gas flow.

(ii) OCR Test 3, Sulfided

This NiO/Al_2O_3 catalyst was reduced by Catalysts and Chemicals, Inc. with 1% H_2S in a H_2 stream. It was later observed to be inactive. The sample was examined in the as-received condition and after etching. The spectra are shown in Figure IV A9. The charge corrected binding energies and details of the etching program are listed in Table 5. The results of the study are noticeably different from those obtained for the C-150-1-01 Run 77 catalyst.

The data for the surface region shows a very low but measurable concentration of sulfur. A much higher signal intensity ratio of S to Ni would be expected for this sample[15] for equal abundances of S and Ni. The surface region appears to be very similar to the unreduced catalyst[1] and may be a nickel-aluminate complex formed during the reduction, testing, and subsequent re-oxidation of the surface.

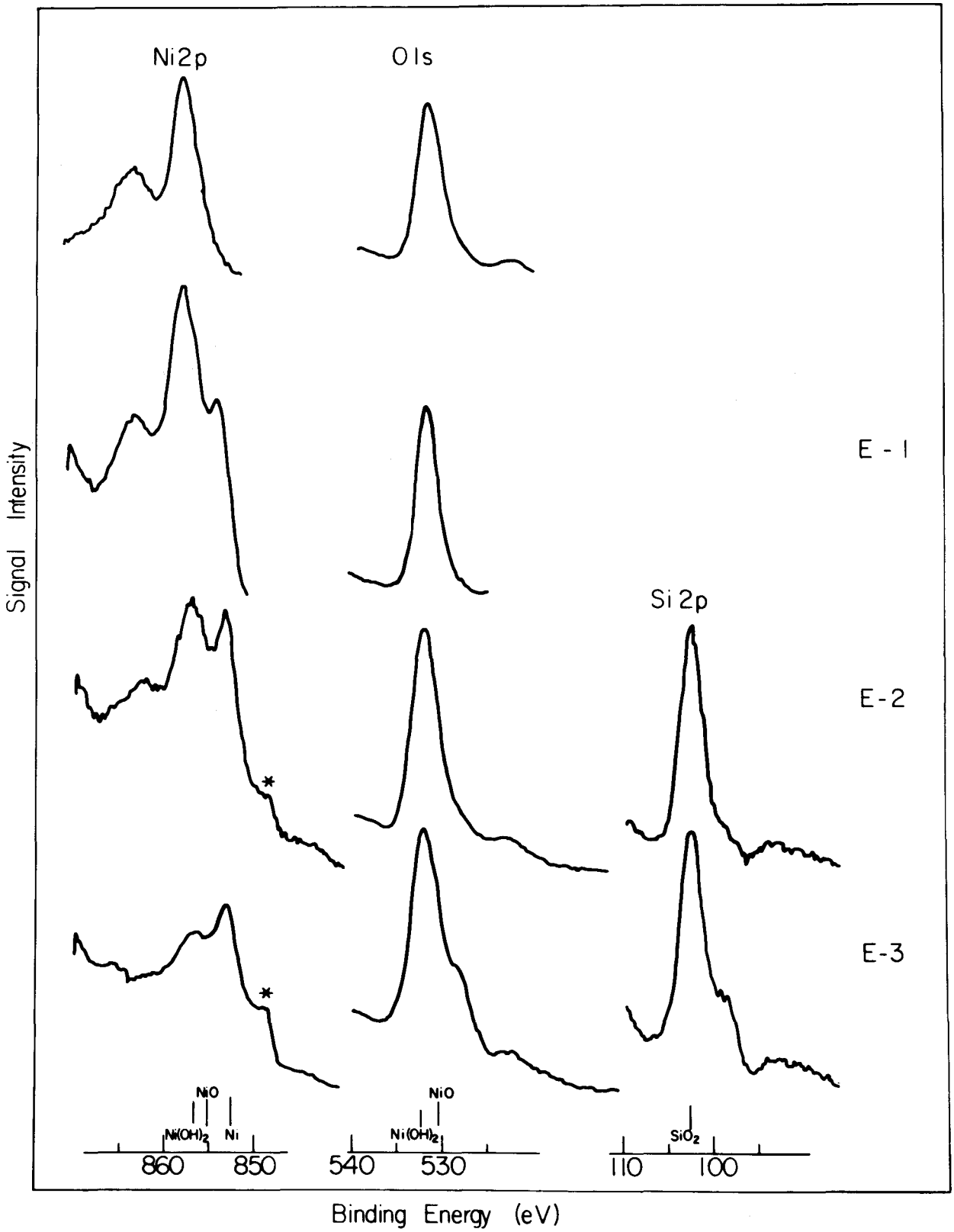

Figure IV A8. ESCA Spectra (Ni $2p_{3/2}$, O $1s_{1/2}$, and Si 2p) of the C150-1-01, Run 77 catalyst before and after a series of etches.

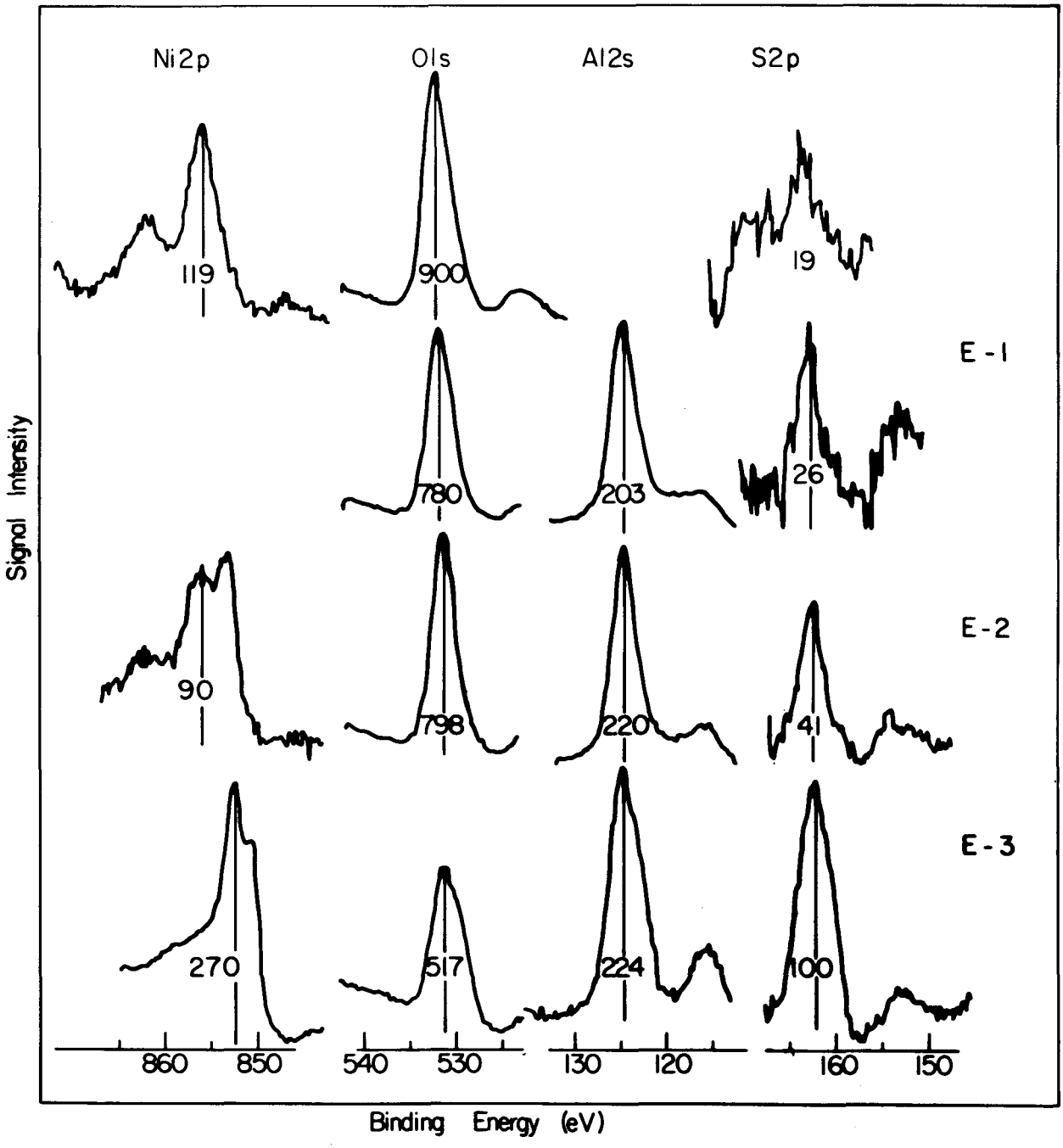

Figure IV A9. ESCA Spectra (Ni $2p_{3/2}$, O $1s_{1/2}$, S2p) of the sulfided OCR Test 3 catalyst. The peak widths and counting rates are also indicated.

The sample was exposed to atmospheric conditions for several months before examination. A spectrum of the Al 2s peak was not obtained during this run.

Following the brief initial etch (E-1), a decrease in the O 1s signal intensity and an increase in the sulfur signal was observed. The binding energies were essentially unchanged. A longer etch (E-2), led to substantial changes in the spectrum. The S 2p peak became stronger, the O 1s and Al 2s peaks were not greatly changed. The Ni 2p spectrum showed a weakened satellite structure and a strong new peak. The binding energy of this peak is similar to that of NiS, but it may be due to nickel metal, there being a small uncertainty in the spectrometer work function forthis set of data. Until other nickel sulfur compounds are examined the exact form of the bonding cannot be specified.

The intensity ratio between sulfur and nickel was found to approach an equal abundance value. Following the final extended etching (E-3), a complex spectrum was observed. The peaks are all broadened. This can be attributed to the sample becoming only partially charged, so that some areas of the surface are uncharged with peaks occurring at the charge corrected positions, and other areas of the surface are charged, with peaks shifted to higher binding energies. The lower O 1s signal intensity is compensated for by the broadening of the peak. The Ni 2p spectrum now has no satellite peak structure and also appears to reflect the partially charged nature of the sample. The spectrum resembles either NiS or Ni metal. Further studies should clarify this interpretation. The S/Ni signal ratio is now quite large suggesting that nearly all free Ni atoms have become bonded to a S atom, thus rendering the catalyst inactive. This suggests that the sulfur pickup has not occured until after reduction of the nickel oxide, NiO being more stable than NiS. The sample reduction thus appears to have been quite

complete as no NiO is observed in the sample bulk. The sulfur penetration into the sample is quite deep as the sulfur intensity increases with the etching. The weak surface region sulfur signal may be due to the replacement of sulfur by oxygen during the extended air exposure.

(ii) Work Forecast

(1) Nickel aluminate and nickel silicate samples will be prepared and examined along with other forms of Ni-S.

(2) The C-150 catalyst series will be reviewed following the installation of the flood gun and using improved sample handling techniques.

(3) Sintered and reduced forms of the L140 catalyst series will be studied to test the model of the signal intensity ratios proposed and to examine the effects of the varying metal loading on the degree of reduction.

(4) The flood gun and gas admission manifold will be constructed and tested. The necessary parts have been delivered or ordered.

(5) The ESCA system will be moved to the Kentucky Center for Energy Research. Downtime of about 3 weeks is anticipated to allow for moving, reassembly, testing and maintenance.

(6) The study of used catalysts will continue.

(7) Tests of a promising sulfur resistant catalyst being developed by Catalysts and Chemicals, Inc. will be initiated.

(8) Studies of gas adsorption on clean catalysts will be initiated, using the gas admission manifold.

(iii) References

(1) P. J. Reucroft, E. B. Bradley, R. J. De Angelis and G. A. Sargent, "Surface Structure and Mechanisms of Gasification Catalyst Deactivation," First Annual Report, February 1, 1976 to January 31, 1977, ERDA Contract No. E(49-18)2229.

(2) J. Haber, J. Stoch, and L. Ungier, J. Elect. Spect. 9, 459 (1976).

(3) H. D. Hagstrum and G. E. Becker, J. Vac. Sci. Technol. 14, 369 (1977).

(4) K. S. Kim and N. Winograd, Surf. Sci. 43, 625 (1974).

(5) R. B. Shalvoy, G. B. Fisher and P. J. Stiles, Phys. Rev B 15, 1680 (1977); contains the binding energies of sulfur and a variety of binary sulfides.

(6) M. Oku and K. Hirokawa, J. Elect. Spect. 10, 103 (1977).

(7) J. S. Brinen, T. L. Schmitt, W. R. Doughman, R. J. Achorn, L. A. Siegel and W. N. Delgass, J. Cat. 40, 295 (1975).

(8) L. H. Scharpen, J. Elect. Spect. 5, 369 (1974).

(9) D. Briggs, J. Elect. Spect. 9, 487 (1976).

(10) A. L. Hausberger, K. Atwood, and C. B. Knight, "Development of Methanation Catalysts for Synthetic Natural Gas Processes," presented at the Symposium on Methanation of Synthesis Gas, Division of Fuel Chemistry (ACS), Atlantic City, New Jersey, September, 1974.

(11) A. L. Hausberger and W. A. Kustes, "Sulfur Resistant Methanation Catalysts," First Annual Report, ERDA Contract No. E(49-18)2032, July 1976.

(12) D. R. Penn, J. Elect. Spect. 9, 29 (1976).

(13) C. J. Powell, Surf. Sci. 44 29 (1974).

(14) J. S. Brinen, J. Elect. Spect. 5, 377 (1977).

(15) J. H. Scofield, Lawrence Livermore Laboratory, Report No. UCRL-51326, Jan. 1973.

Table 1

Corrected Binding Energies (eV) for $Ni(OH)_2$ and NiS

$Ni(OH)_2$	Binding Energy	FWHM(eV)
Ni $2p_{3/2}$	856.6	3.6
Satellite	862.3	
O $1s_{1/2}$	532.2	2.3

Charging ~2.4 eV

NiS	Binding Energy	FWHM
Ni $2p_{3/2}$	853.2	1.6
Satellite	855.7	
S $2S_{1/2}$	226.4	3.2
S 2p	161.6	2.5

No Charging Observed

Table 2

Experimental and Calculated $R(\frac{Ni}{Al})$ Intensity Ratios

Sample	Nickel Wt. Percent	Atomic Abundance		$R(\frac{Ni}{Al})$	
		Ni	Al	Exp.	Calc.
L141	10	0.04	0.37	0.29	0.25
L142	20	0.08	0.34	0.45	0.59
L143	30	0.13	0.30	0.92	1.07
L144	40	0.18	0.26	1.61	1.79
C150-1-03	47.5	0.23	0.22	1.91	2.64

Table 3

L140 Catalyst Binding Energies (eV)

	L141		L142	
Etch Time (min)	0	30	0	30
Ni 2p	856.7	856.8	857.2	857.2
O 1s	531.9	531.7	532.2	532.1
Al 2s	119.4	119.7	120.2	120.2

	L143		L144	
Etch Time (min)	0	30	0	30
Ni 2p	856.4	856.7	857.3	857.0
O 1s	531.6	531.9	532.2	531.8
Al 2s	119.4	119.7	120.1	119.9

Charging was typically 4 eV.

Table 4

Etching Program and Binding Energies (Charge Corrected): Run 77 C150-1-01

Etch #	0	1	2	3	Std (Ni-Si)
Ni 2p	862.6	862.1	862.3		
	856.7	857.2	856.8	856.9	856.7
		853.8	853.3	853.2	
			852.8	852.8	
O 1s	532.3	532.8	532.3	532.3	532.5
				532.0	
Si 2p			102.8	102.9	
Etching (min) Time	0	10	20	40	

Ni, O compare with both Ni-Si or $Ni(OH)_2$

Charging ~ 4 eV

Table 5

Etching Program, Binding Energies (Charge Corrected), and Peak Signal Ratios (to O 1s): OCR Test 3

Etch #	0	1	2	3
Peak				
Ni 2p	861.8	-	861.6	-
	856.7	-	856.1	-
			853.5	852.5
				853.4
O 1s	531.4	531.4	531.4	531.4
Al 2s		119.6 (.26)	119.8 (.30)	119.7 (.43)
S 2p	163* (.02)	162.5 (.04)	162.4 (.06)	162.2 (.20)
Etch Time (min)	0	.33	5	35

*weak signal

Charging ~3 eV

B. REPORTING CATEGORY 2 - LASER RAMAN AND INFRARED SPECTROSCOPY (Prepared by J. M. Stencel and E. B. Bradley)

(i) Work Accomplished

The Ar^+ laser has been installed and Raman studies of the methanation catalysts begun while the UHV-gas adsorption chamber is being completed. The laser, which is discretely tunable from 4579 to 5145A^o, should allow a variety of colored samples to be studied without their photodecomposition. However, the catalyst samples are black and hence absorb all wavelengths within the visible spectrum. Consequently the scattered Raman intensity is greatly reduced from that of a white sample and, as discussed below, special sampling techniques, scattering geometry, laser intensity and laser light focal properties are necessary. We also provide in this report the Raman spectra of the Al_2O_3 and SiO_2 support materials in order to provide a basis for the interpretation of the catalyst spectra.

Analysis of Raman Data

a) SiO_2

The sampling techniques used for this spectrum and others in this report consisted of packing the powdered samples in 1mm diameter capillaries and sealing the ends, or packing the powder in one end of a brass cylinder. All spectra were obtained with 90^o scattering; the geometry of the incident and collected scattered light with respect to the samplers is shown in Figure IV B1.

(a) Capillary (b) Brass Holder

Figure IV B1. Scattering geometry used for obtaining Raman spectra; α is the angle of incidence.

These holders were attached to a goniometer which allowed a controlled incident beam angle α. Collecting efficiency could be increased in some cases for the brass sampler by decreasing α which increased the amount of sample illuminated while producing a line image on the monochromator entrance slit. Decreasing α beyond approximately 15^{o} for the glass capillary did not increase the Raman signal. This result can be explained in terms of increased reflectivity losses at the glass-air interface as α tends to 0^{o}.

Figure IV B2 shows the Raman spectrum of powdered SiO_2 from 0 to 4000 cm^{-1} using the glass capillary for sample containment and 3

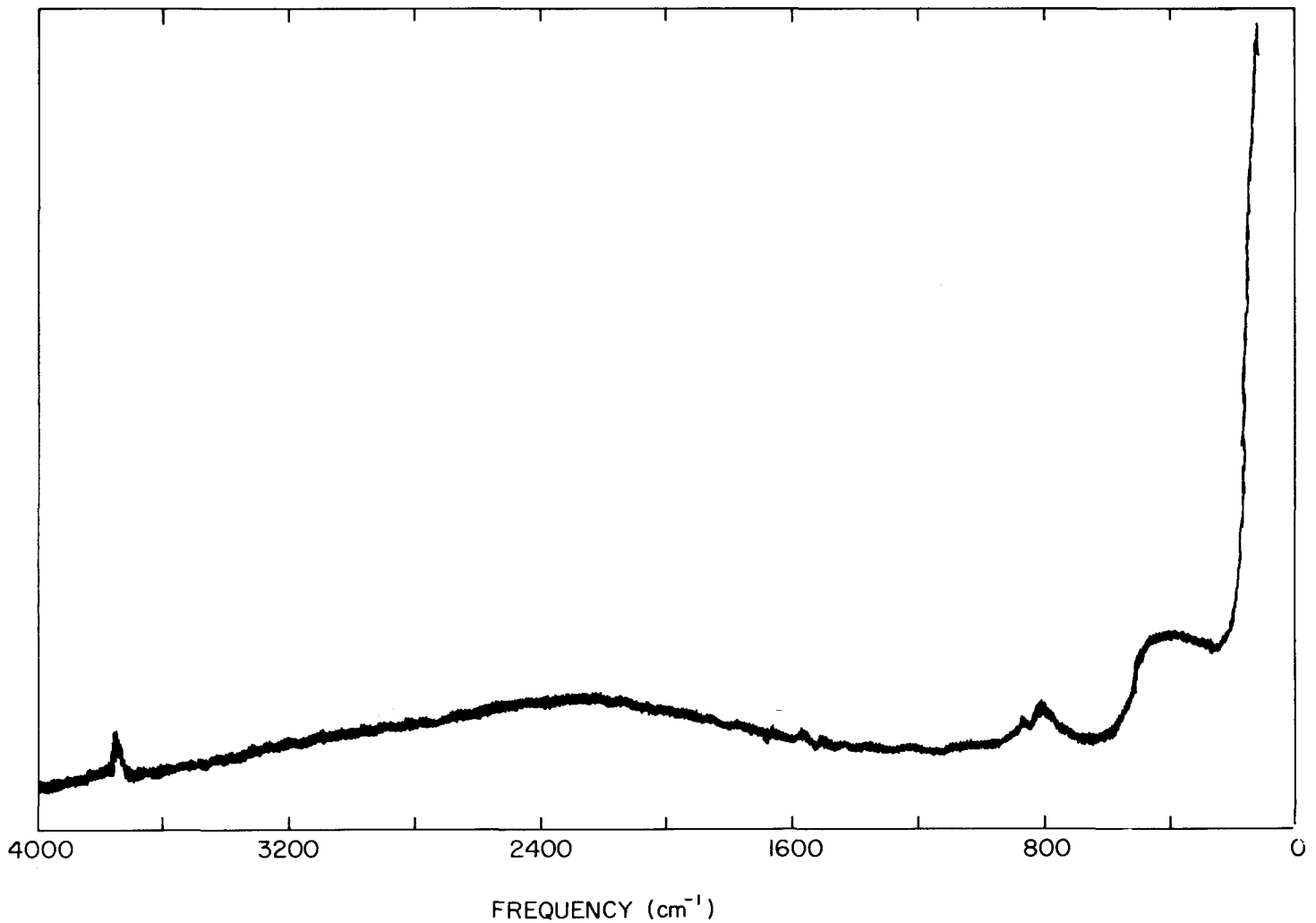

Figure IV B2. Raman spectrum of powdered SiO_2.

Watts incident power at 5145A^{o}. A reference spectrum of the capillary without SiO_2 showed only the broad band structure centered at 400 cm^{-1}. SiO_2 spectra obtained while using the brass sampler were identical to that of Figure IV B2 except the broad 400 cm^{-1} band had decreased intensity. This reference spectrum indicates that the capillaries are essentially silica complexs and can be used as sample holders without serious problems of spurious Raman lines. The other spectral details of note are the 810 cm^{-1} band and a shoulder at 860 cm^{-1}, a narrow band at 3735 cm^{-1} and the very broad-humped contour which is centered at approximately 2200 cm^{-1}.

The C_{2v} symmetry of SiO_2 should allow 3 Raman bands. However, silicon oxide rarely exists in bulk form as SiO_2 molecules except in quartz. Hibben shows that Raman bands for SiO_2 are located from 215 to 500 cm^{-1}, 600 to 800 cm^{-1} and 915 to 1200 cm^{-1}.[1] The former 2 regions produce the most intense Raman scattering while the latter is approximately 0.1 as intense. The abscence of Raman bands in the 1000 cm^{-1} region for our sample could be partially explained in terms of the inherent low intensity of these bands. The broad nature of those bands that are seen indicates the SiO_2 is amorphous which would also decrease the band intensities.

The 3735 cm^{-1} band is most likely an Ar^{+} plasma emission line. This band is also evident in the $NiCO_3$ spectrum (see below) which would not be expected if it was due to adsorbed OH^{-} attached to surface Si atoms. Its frequency agrees with that for a plasma emission line as noted by Loader,[2] except its intensity is large compared to his values. The band origin could be exactly determined by using a laser narrow

band-pass filter for the 5145A^{o} line or by obtaining spectra using different exciting wavelengths. However, we do not yet have the necessary filters and the number of strong plasma lines increase with decreasing laser wavelengths causing more difficult spectral interpretation.

The very broad contour centered at 2200 cm^{-1} is due to fluorescence. This type of emission background has been noted to be weak in silica compounds and strong in aluminas and silica-aluminas.[3] In extreme cases this emission background can be orders of magnitude greater in intensity than the Raman lines. Various mechanisms have been proposed to explain this phenomena and to reduce effectively its Raman obscurring effect.[4] The SiO_2 fluorescence is not large compared to that found for some $NiCO_3$ samples (see below).

b) Al_2O_3

The Raman spectrum of powdered Al_2O_3 is shown in Figure IV B3. It is the average of 3 spectral runs using 3 watts exciting power at 5145A^{o} with the Al_2O_3 sample packed in the brass sampler. Weak bands are seen on the edge of the Rayleigh line at 315, 360, and 390 cm^{-1} and a broad band appears at 460 cm^{-1}. According to Porto *et al.*[5] and Ashkin *et al.*[6] crystalline Al_2O_3 should have Raman bands at 378, (418, 432, 451), 578, 645 and 751 cm^{-1}. Figure IV B3 indicates that the 400 to 500 cm^{-1} region has the greatest intensity which could be due to the combination of the crystalline 418, 432 and 451 cm^{-1} bands. Other Raman band frequencies of our Al_2O_3 sample do not correspond to the above published values. However, our sample is an amorphous solid,

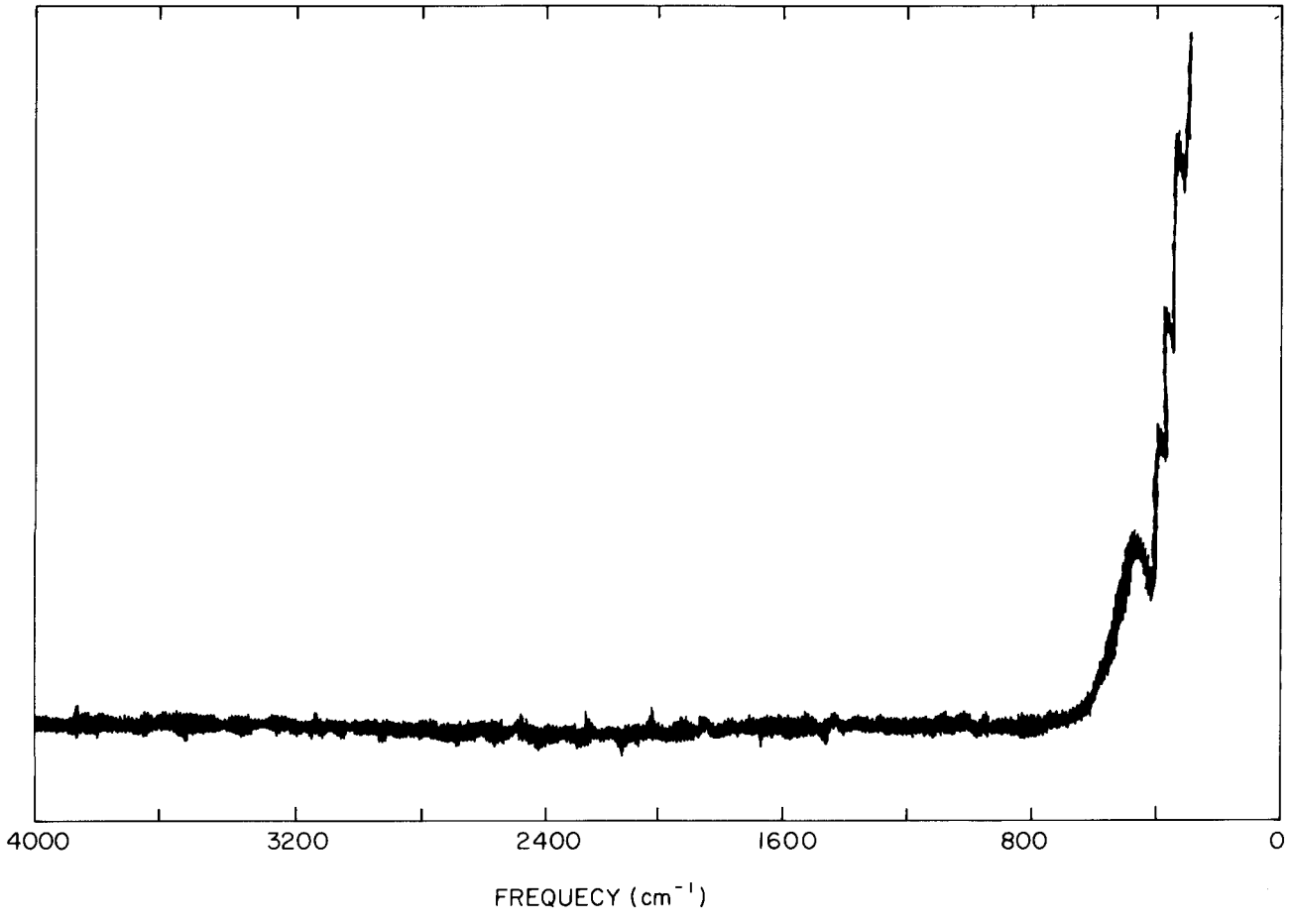

Figure IV B3. Raman spectrum of powdered Al_2O_3.

and as such, should possess weak Raman scattering not necessarily at the same frequencies as that for crystalline Al_2O_3.

c) $NiCO_3$

The Raman spectra of 2 different $NiCO_3$ samples are shown in Figure IV B4; each is an average of 2 spectral runs using 500 mW of unfocused incident light at 5145A°. Strong fluorescence is noted in one spectrum which is not readily explainable since both samples had similar preparation and handling. In each spectrum bands are evident at 1075, 1117, 1690, 2422 and 3735 cm^{-1}. The 3735 cm^{-1} band is due to Ar^+ plasma emission.

The most intense Raman band should be associated with the symmetric C-O stretch which would be expected in the 1060 to 1150 cm^{-1} region.[7,8] We assume that the strong 1117 cm^{-1} band is associated with this vibration. Doublet structure in this region could be due to hydrogen bonding. Such bonding would produce a characteristic broad contour while the C-OH Raman band should appear near 1050 cm^{-1}.[8] However, no C-H bands are seen near 2900 cm^{-1}. Likewise the symmetric C^{13}-O stretch would produce a band near 1072 cm^{-1} if that at 1117 cm^{-1} is due to the C^{12}-O stretch. However, the natural abundance of C^{13} is considered too small to produce a band with approximately 1/2 the intensity of the C^{12}-O stretch. An alternate possibility which could explain the 1700 to 1000 cm^{-1} region is that the $NiCO_3$ is composed of both monodentate and bidentate $CO_3^{=}$ species. The 1690 cm^{-1} band would then be due to C = O stretching and the 1075 cm^{-1} band due to C - O stretching of the bidentate species while that at 1117 cm^{-1} would still be associated with the

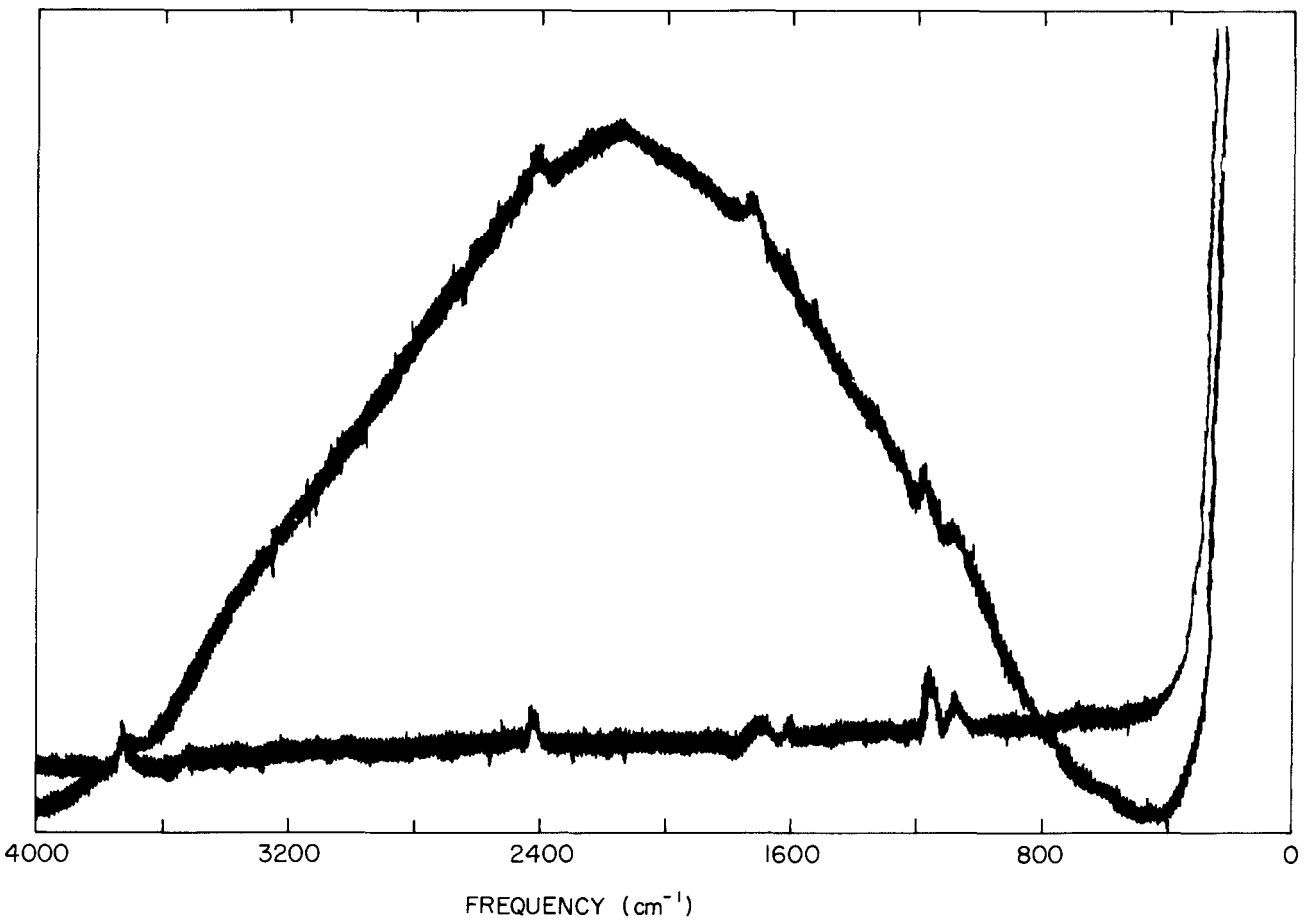

Figure IV B4. Raman spectra of two different $NiCO_3$ samples. The fluorescence background for one of the samples is not readily explainable.

C - O stretching of the monodentate species. Such an explanation would be based on the partial photodecomposition of the monodentate carbonate, which is seen in infrared studies[9], to bidentate carbonate. Photodecomposition is possible, as discussed below, but no time-dependent intensity studies were performed to determine whether the 1690 and 1075 cm^{-1} bands became more intense at the expense of the 1117 cm^{-1} band. The other $NiCO_3$ band at 2422 cm^{-1} has been explained previously in terms of overtones.[7] Such an explanation would be possible only if the site symmetry of the molecule was such that the fundamental was inactive or very weak. Typically the overtone and combination bands are 0.01 as intense as the fundamentals.

Infrared studies have shown that the monodentate carbonate species decomposes with heat to form NiO and CO_2.[9] $NiCO_3$ is yellow-green and absorbs in the blue-green spectral region which is the lasing region of the Ar^+ laser. More than 500 mW unfocused, or 100 mW focused, 5145A° light would pyrolyze the $NiCO_3$. The black compound produced from this action was determined from infrared studies to be NiO. Infrared results of a similar type of photodecomposition is seen in the spectra shown in Figure IV B5. Comparing these spectra we find that the carbonate does not form carboxylate species when laser treated and that the H_2O does not evolve as in the heating experiment. Increased absorption near 440 cm^{-1} for the laser treated sample indicates NiO formation while increased absorption near 500 cm^{-1} for the heated sample indicates Ni - C bond formation.

$\underline{NiSiO_3}$

Figure IV B6 shows the Raman spectrum of the green $NiSiO_3$ sample. It

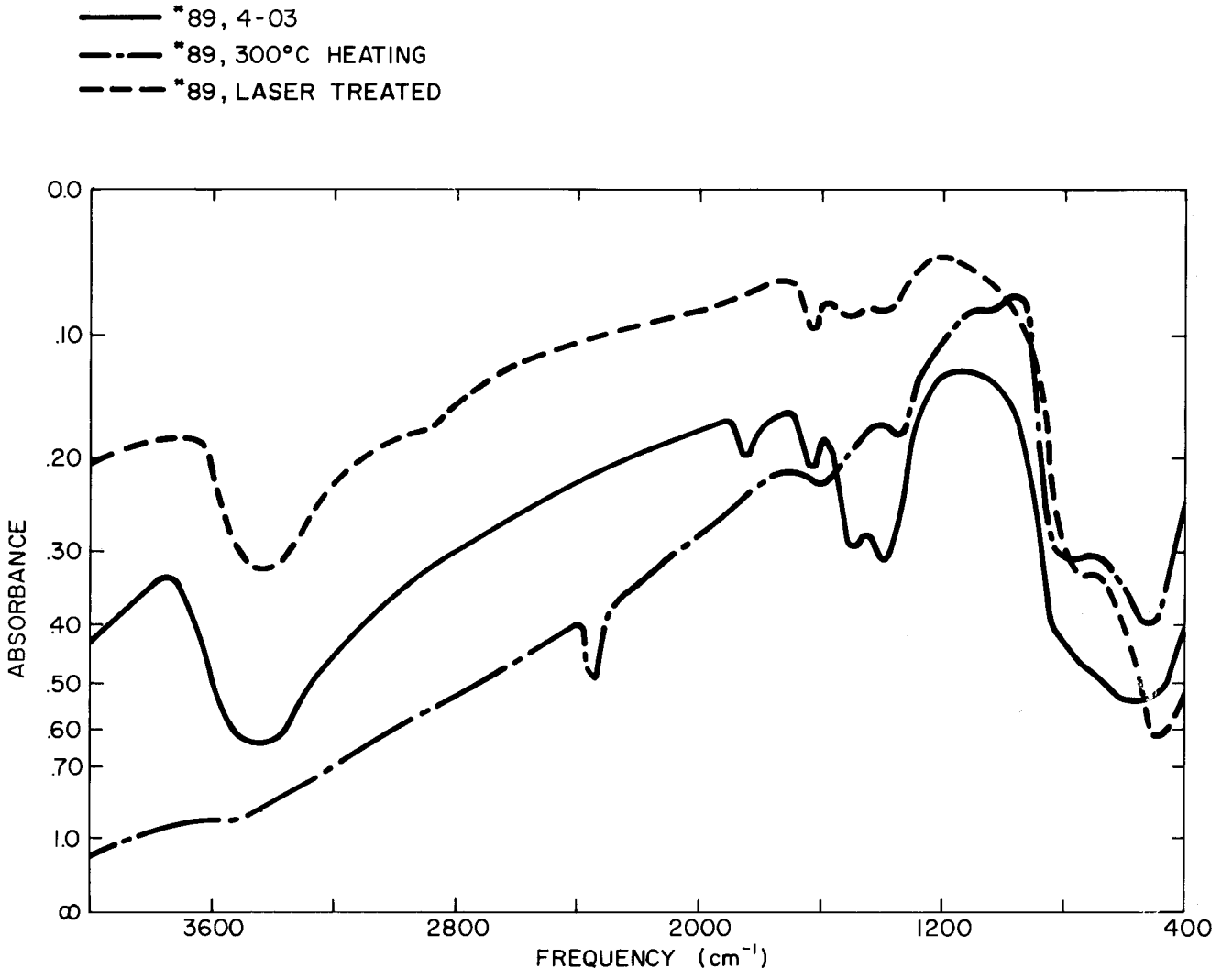

Figure IV B5. The infrared spectrum of Run #89, C150-4-03 compared to its spectra after heating at 300°C and laser exposure for 3W incident power at 5145 Å.

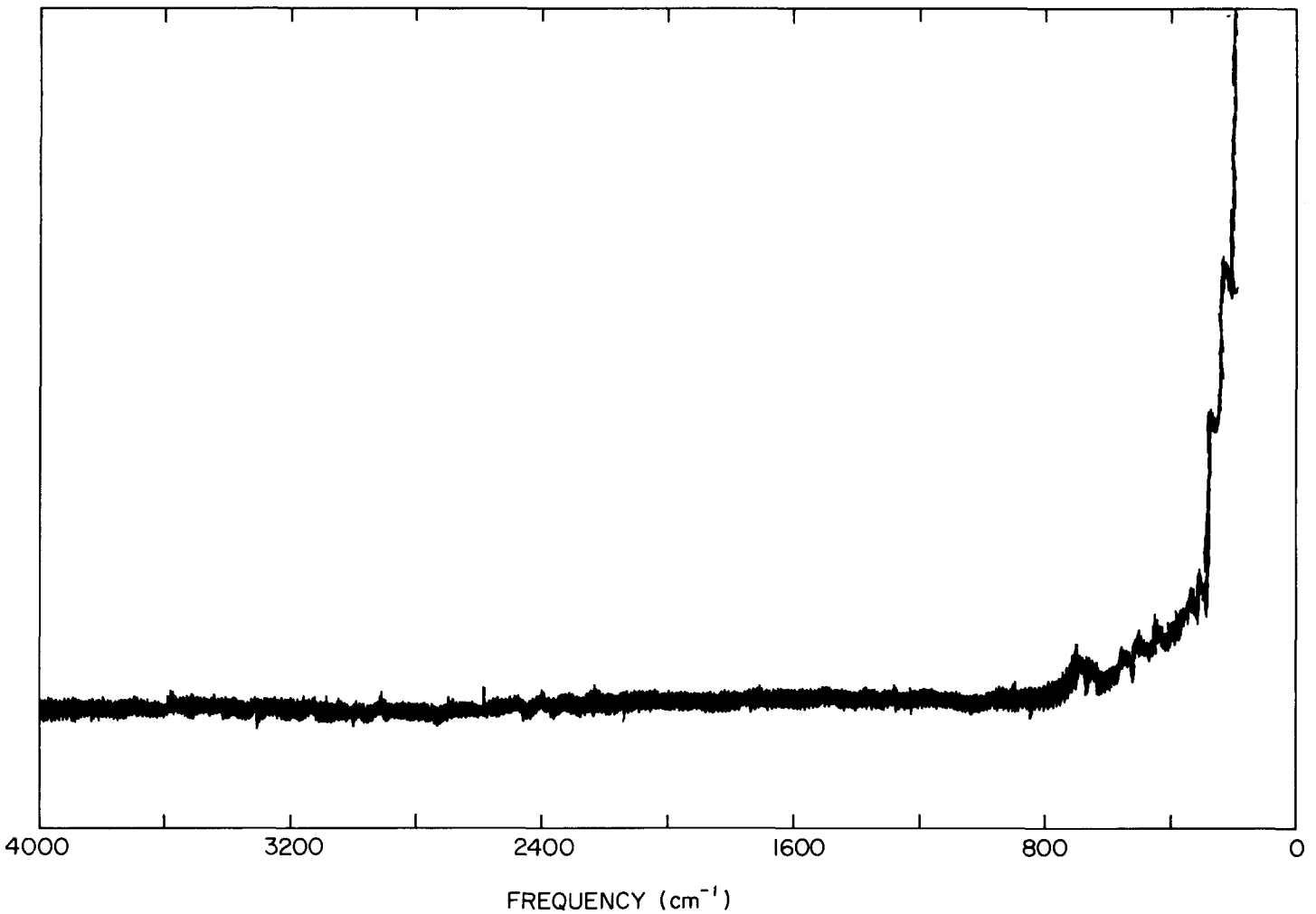

Figure IV B6. Raman spectrum of powdered $NiSiO_3$.

is an average of 3 spectral runs using 500 mW of unfocused light at 5145A°. Weak Raman bands are located at 215, 254, 285, 302, 420, 478, 607 and 652 cm^{-1}.

High incident laser power would decompose the $NiSiO_3$ sample as was found for $NiCO_3$. Consequently unfocused laser light, large spectral slit-widths, high detector gain and repeated scanning was necessary in order to locate the weak Raman bands. This weak scattering is characteristic of amorphous silicas (and aluminas) and it allows the 0 to 4000 cm^{-1} spectral region to be used for interpretation of adsorbed species as compared to the intense adsorbent bands seen in the infrared spectra.[10,11]

Sulphided Catalyst

This is the sulphided alumina-support catalyst of which infrared spectra had previously been obtained.[11] Its Raman spectrum, shown in Figure IV B7, has bands located near 310, 350, 410, 500, 585, 817, 1028, 1130, 1310, 1380, 1415, 1525 and 1620 cm^{-1}. It is the average of 3 spectral runs using the 5145A° exciting line with 600 mW of unfocused light. Approximately 3 W/cm^2 would transform the extremely black-colored sample to one of green-gray.

Ross[12] shows that the prominent Raman bands of $NiSO_4$ are near 430, 620, 980 and 1120 cm^{-1}, while Hibben[13] assigns bands near 460, 610 and 980 cm^{-1} to $SO_4^=$ vibrations of $Al_2(SO_4)_3$. In addition, the $SO_4^=$ species in solution gives Raman bands at 450, 610, 980 and 1100 cm^{-1} while the $SO_4^=$ vibrations in H_2SO_4 are located near 310, 560 and 1140 cm^{-1}. Similarly, monodentate and bidentate sulphite complexs give rise to Raman bands at the same frequencies[14]. The strong 1130 cm^{-1} band and the 1028 and 310 bands

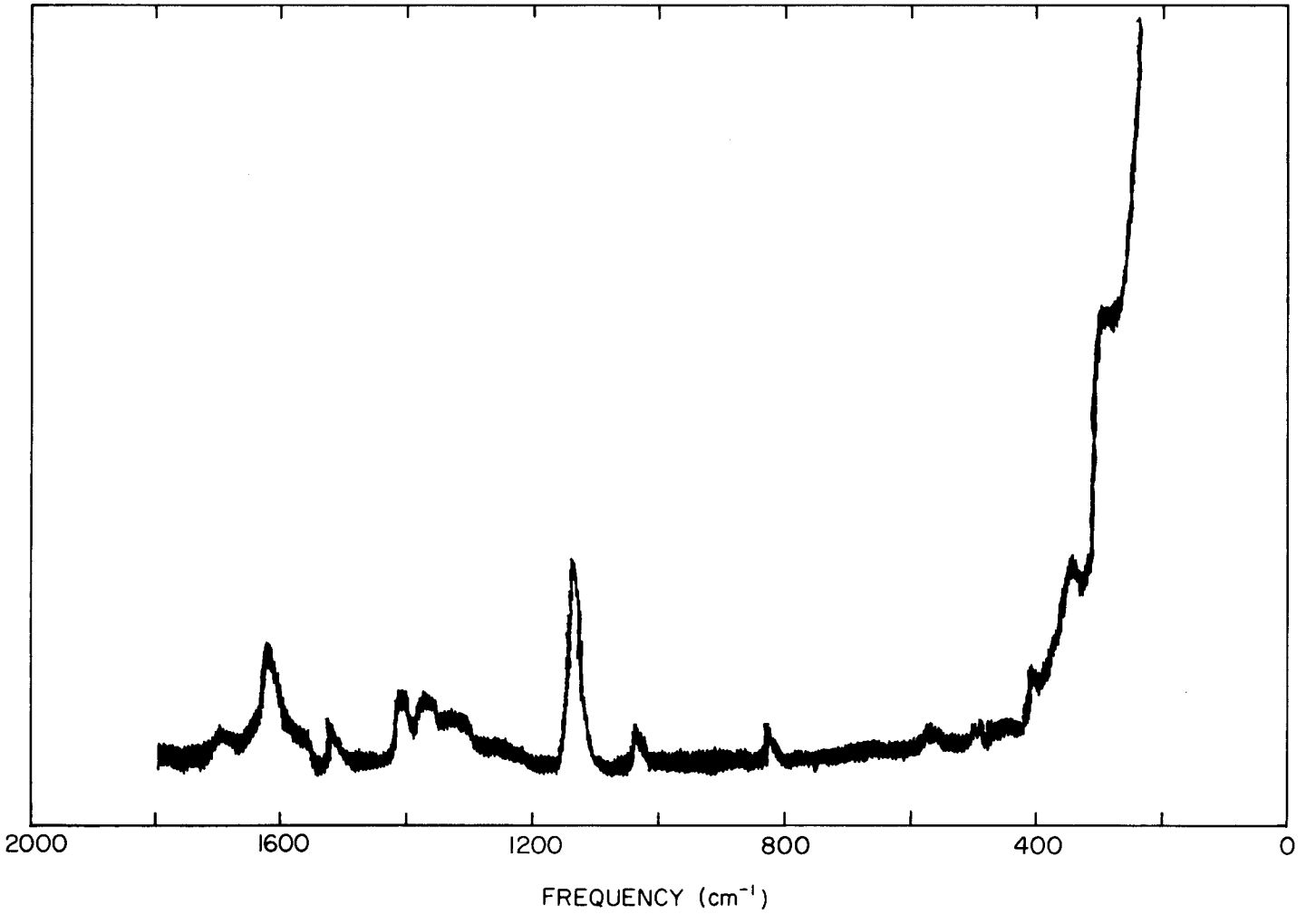

Figure IV B7. Raman spectrum of sulphided C150-4-03 catalyst from 0 to 1800 cm^{-1}.

are thus believed to be due to sulphate or sulphite vibrations since their frequencies and intensities are indicative of such species. Other assignments are more tentative because Figure IV B7 is the result of preliminary studies. However, it is known that the largest S - O Raman frequency would be located near 1400 cm^{-1}. This location implies the complex structure between 1300 to 1400 cm^{-1} could be the result of thionyl complexs. It is also possible that the presence of carbon in the catalysts and the synthesis gas stream, along with sulfur and subsequent oxidation, would produce C = S, C = C, C = O and C - O binding. The C = S bond frequency, located at 850 cm^{-1} for carbon oxysulfide, could be at 817 cm^{-1} while the 1620 cm^{-1} band could be the result of C = C stretching. Also, the 1300 - 1400 cm^{-1} structure could be caused by C - O vibrations from $CO_3^{=}$ or CO_2^{-} species. Definitely more Raman spectra are necessary to define the spectral characteristics of the sulphided catalyst. Also, the Raman spectra of C150-4-03 and C150-1-03 catalysts should be studied before synthesis gas exposure and after they have been exposed to carefully controlled gas adsorption experiments.

(ii) Work Forecast

The Raman spectra of the SiO_2 and Al_2O_3 catalyst support materials show very weak-broad bands which are indicative of an amorphous solid. No Raman active OH^- vibration was found as in the infrared,[9] while weak Raman scattering is opposite to the intense infrared absoprtion observed for SiO_2 or Al_2O_3. The Raman spectra of the NiO/Al_2O_3 or NiO/SiO_2 catalysts should also show weak bands since the ionic character of the NiO bonding should not induce Raman active vibrations. However, we have not completed studies of these catalysts since their black color increases substantially the difficulty of obtaining accurate-repeatable spectra. Preliminary spectra indicate these

spectra will be simple except for band associated with the carbon which is used as a binder.

The $NiCO_3$ and $NiSiO_3$ spectra are also relatively simple. Strong fluorescence that is seen in some samples is not readily explainable unless surface contamination resulted from different unknown handling procedures. Fluorescence was not excessive for SiO_2 or Al_2O_3 and preliminary studies show it will not hamper substantially the study of the catalysts. Careful control of incident laser power will be necessary however, since we have shown possible changes in infrared spectral characteristics due to photodecomposition. This type of pyrolysis leads to carbonate decomposition and NiO formation in synthesis-gas-exposed catalysts without the removal of bound H_2O.

The Raman spectrum of the sulphided catalyst is complex but we have been able to identify adsorbed sulphate or sulphite species. It is not known whether the S-O bands are the result of an aging mechanism or whether they result from the oxygen which is present in the synthesis gas stream. More studies will be performed in which the spectra of unused catalysts will be compared to those that have been sulphided and those which have been shown to have adsorbed intermediate methanation products.[11] Simultaneously, we will be completing our experimental gas adsorption system so that studies on crystalline Ni surfaces can be initiated.

(iii) References

(1) J. H. Hibben, The Raman Effect and its Chemical Applications, American Chemical Society Monograph Series, p 410.

(2) J. Loader, Basic Laser Raman Spectroscopy, (Heyden & Son, Ltd., 1970) pp. 32-35.

(3) P.J. Hendra and E.J. Loader, Trans. Faraday Soc. 67, 828 (1971).

(4) R.P. Cooney, G. Curthoys and Nguyen The Tam, Advances in Catalysis, Vol. XXIV (Academic Press, Inc., New York, 1975) p. 293.

(5) S.P.S. Porto and R.S. Krishnan, J. Chem. Phys. 47, 1009 (1967).

(6) M. Ashkin, J.H. Parker, Jr. and D.W. Feldman, Solid State Comm. 6, 343 (1968).

(7) Reference 1, p. 428.

(8) S.D. Ross, Inorganic Infrared and Raman Spectra, (McGraw-Hill Book Co., 1973) pp. 159-166.

(9) P.J. Reucroft, E.B. Bradley, R.J. DeAngelis and G.A. Sargent, Quarterly Report No. 3, "Surface Structure and Mechanisms of Gasification Catalyst Deactivation", August 1 to October 31, 1976, ERDA Contract No. E(49-18) 2229, pp. 37-39.

(10) Reference 9, pp. 31-52.

(11) P.J. Reucroft, E.B. Bradley, R.J. DeAngelis and G.A. Sargent, Quarterly Report No. 4, "Surface Structure and Mechanisms of Gasification Catalyst Reactivation", November 1 to January 31, ERDA Contract No. E(49-18) 2229.

(12) Reference 8, p. 214.

(13) Reference 1, p. 397.

(14) Reference 8, pp. 177-183.

C. REPORTING CATEGORY 3 - SURFACE ANALYSIS BY LOW ENERGY ELECTRON DIFFRACTION (LEED) AND AUGER ELECTRON SPECTROSCOPY (AES) (Prepared by C. H. Huang and G. A. Sargent)

(i) Work Accomplished

In the previous report,[1] Auger analysis of Ni catalysts (as received, without any attempt of cleaning) was taken. The Ni content was found to have a 20% surface inhomogeneity. The Ni Auger intensity increased rather consistently with the stoichiometric Ni content of the catalysts. Models of the catalyst particles were discussed.

The present study employed argon ions for surface cleaning as well as depth analysis of the elemental distribution of the Ni catalysts. The previous models were further discussed based on the present results. In the meantime, a crystal holder for the LEED specimens, which allows direct ohmic heating, was designed and made. The crystal holder will be used for the study of sulfur poisoning on a single crystal surface. A circuit,[2] which has the feature of constant temperature control and allows the observation of LEED structure at the elevated temperature, was studied and simplified. It is scheduled to be made in the next quarter.

Figure IV C1 and C2 show the intensity variation of C, O, Ni, Al Auger peaks with depth during the Ar^+ bombardment on CCI-L141, CCI-L142, CCI-L143, CCI-L144 and C150-4-03 catalyst samples. The intensity change varies randomly with respect to the Ni content. However, as shown in Figure IV C3, Ni and Al tends to increase in intensity after bombardment. The intensity increase is greater for Ni than Al. Oxygen decreased in intensity by about 10% after bombardment. The carbon intensity was found to change quite randomly, although in most cases, it decreased in intensity.

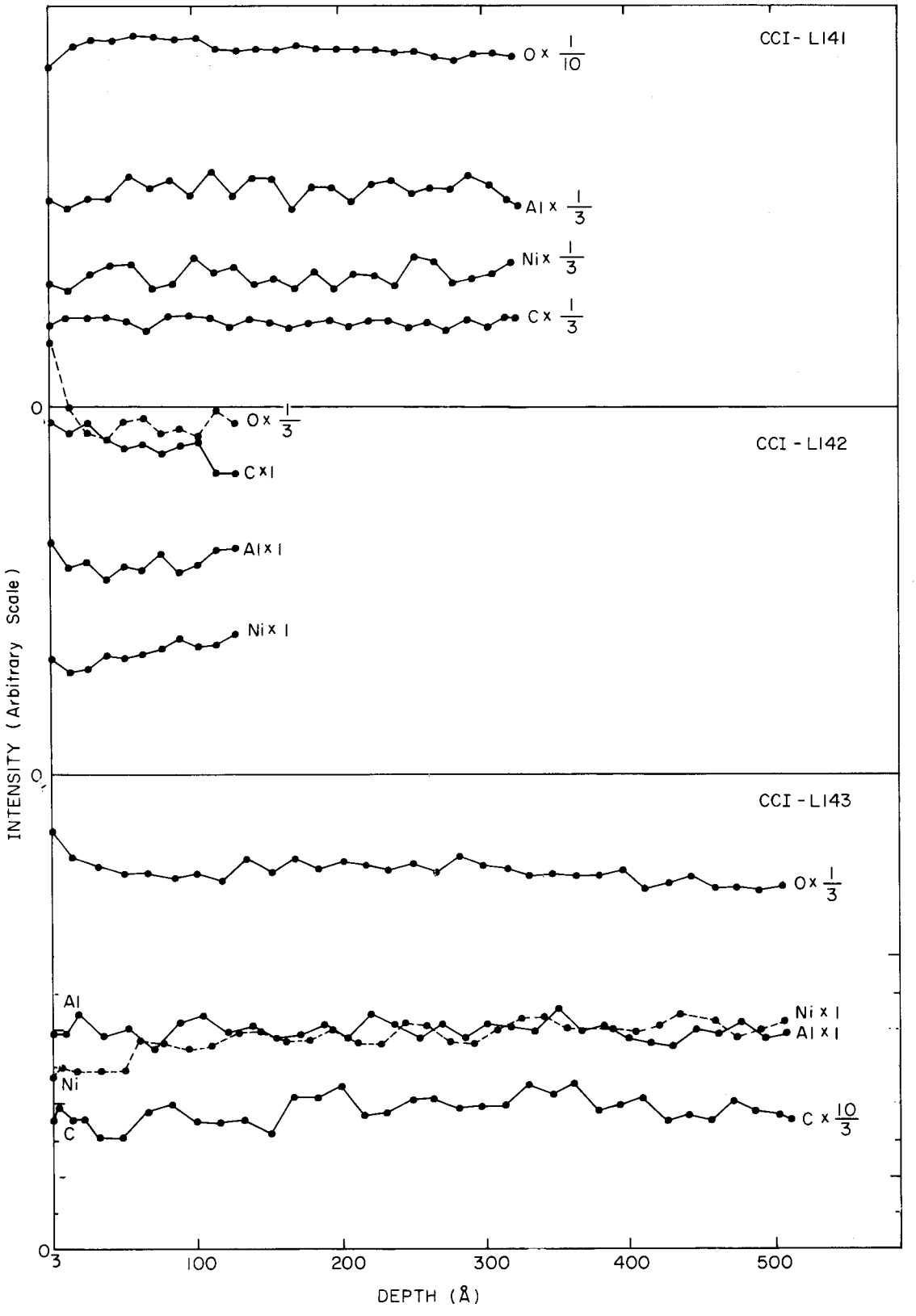

Figure IV C1. Intensity variation of C, O, Ni, and Al Auger spectra during argon ion bombardment on CCI-L141, CCI-L142 and CCI-L143 catalyst samples.

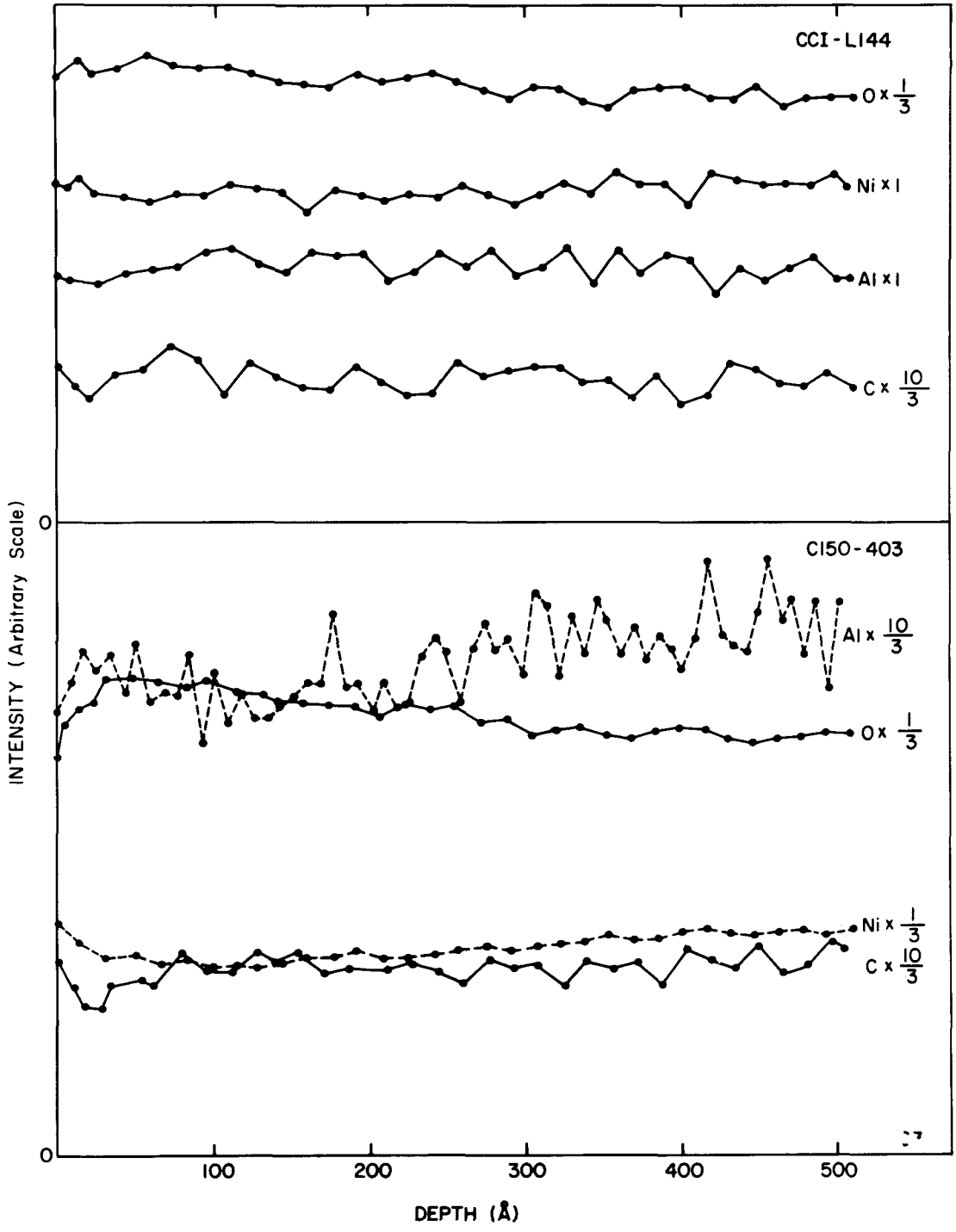

Figure IV C2. Intensity variation of C, O, Ni, and Al Auger spectra during argon ion bombardment on CCI-L144 and C150-4-03 catalyst samples.

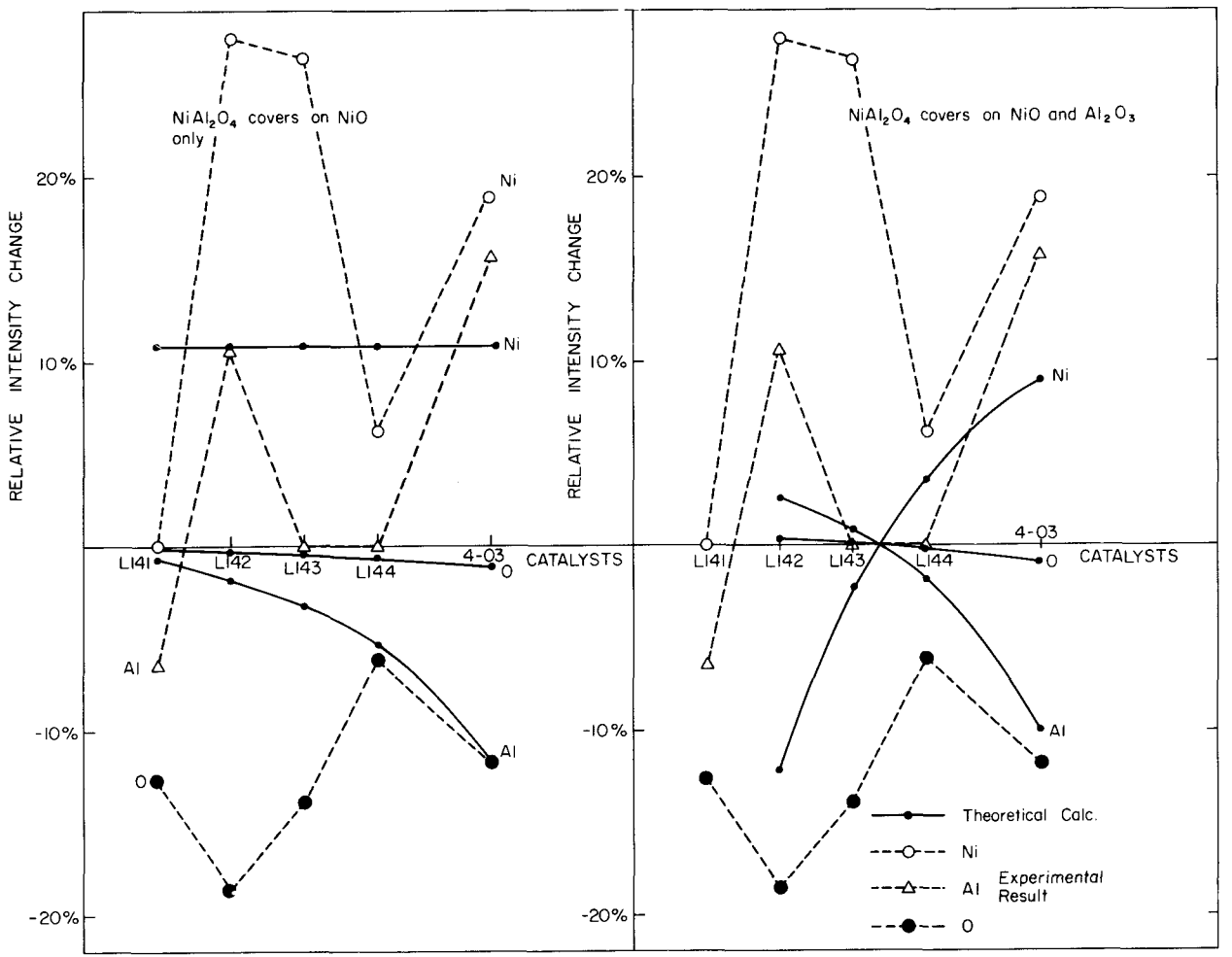

Figure IV C3. Intensity change of Ni, Al, O, C after Ar^+ bombardment vs. Ni content.

(a) Comparison of experimental results with theoretical calculation assuming the formation of monolayer $NiAl_2O_4$ on NiO particle only.

(b) Comparison of experimental results with theoretical calculation assuming the formation of monolayer $NiAl_2O_4$ on NiO and Al_2O_3 parricles.

A complete scan of the Auger spectrum was taken before and after Ar^+ bombardment, as shown in Figure IV C4. The sodium Auger peak was completely eliminated after Ar^+ bombardment, while the creation of an argon Auger peak was presumably introduced by the bombardment (the spectrum was taken with Ar^+ on to maintain a clean surface). Sulfur was found to be still present after removing ~500Å. It is thus believed to be introduced during the preparation of the catalyst. A further investigation of peak shape was performed before and after Ar^+ bombardment by taking narrow scan of C, O, Ni and Al. No appreciable change was found.

Discussion

As shown in Figure IV C1 and C2, a thickness of ~400Å must be removed before the Auger intensity of O, Ni and Al remains relatively constant. Since the average particle size is about 35Å,[1-3] the variation of Auger intensity through the depth of 400Å is most probably due to surface contamination which is caused by the exposure to the atmosphere and handling of these catalysts pellets. This deep contaminated layer could be one of the many reasons which gives rise to the incomplete reduction of these Ni catalysts. The idea of surface contamination is further supported by the big reduction of the oxygen Auger intensity and the drastic increase of Ni and Al Auger intensities. The Auger electron mean free path is about 9Å.[4,5] Previous ESCA and reduction work had indicated the possibility that the NiO particles might be encapulated in a $NiAl_2O_4$ shell. A theoretical calculation of the intensity change of Ni, Al and O is shown in Figure IV C3 A and B. Figure IV C3A assumed the formation of a monolayer of $NiAl_2O_4$ only on NiO particles. Figure IV C3B assumed the formation

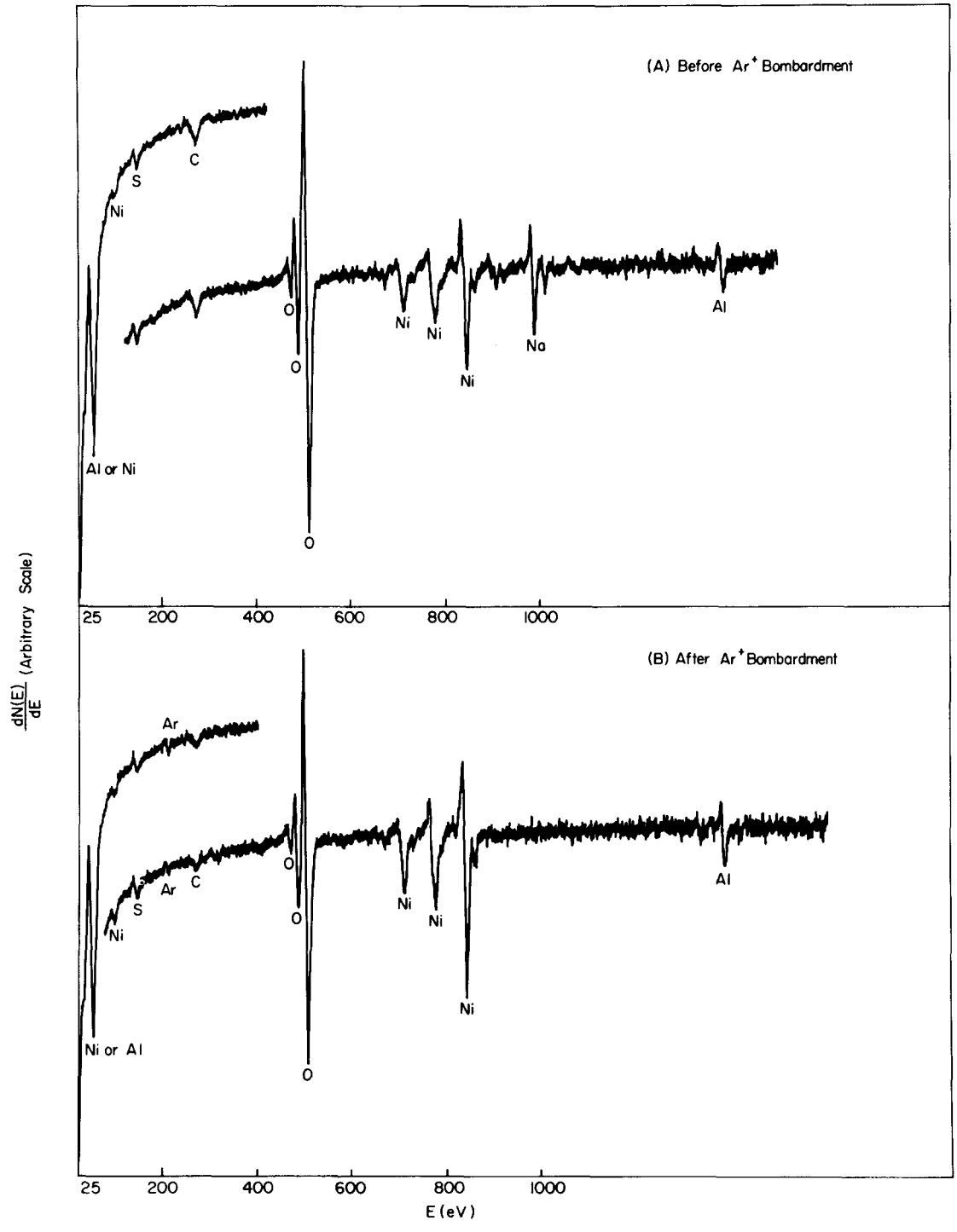

Figure IV C4. Complete Auger spectrum of C150-4-03 catalyst before and after argon ion bombardment.

of a monolayer of $NiAl_2O_4$ on both the NiO and Al_2O_3 particles. The oxygen intensity was expected to reduce by less than 1% in both cases. However, the oxygen intensity was found to be reduced by as much as 6% to 19%. If all the NiO particles were fully covered with a $NiAl_2O_4$ shell, then a 10.8% increase in the Ni Auger intensity would be expected, independent of the Ni content, and the Al Auger intensity should decrease. If $NiAl_2O_4$ covered NiO as well as Al_2O_3 then, depending on the Ni content, either element could decrease or increase in intensity after bombardment. Thus, the present experiment results show little or no correlation with either of the two theoretical models.

The inhomogeneity of the catslysts has made the present study rather difficult. The random variation of Ni and Al intensity with respect to the nickel content could be attributed to this reason. The greater increase in the Ni Auger intensity compared to that for Al has indicated that NiO was more susceptible to the contamination (which most probably is H_2O).

The use of Auger intensity to monitor the Ni content in the catalyst pellet was proven to be promising. After Ar^+ bombardment, the relative Ni Auger intensity varies consistently with the stoichiometric Ni content and is independent of the support material (Al_2O_3 or SiO_2). The result is shown in Figure IV C5. The deviation is about 15% which is mostly due to the surface inhomogeneity and charge up effect.

(ii) Work Forecast

(1) Structure analysis of Ni, Al, O Auger peaks for the unused catalysts and the sulfur poisoned catalyst will be made.

(2) Estimate the sulfur content in the sulfur poisoned catalyst.

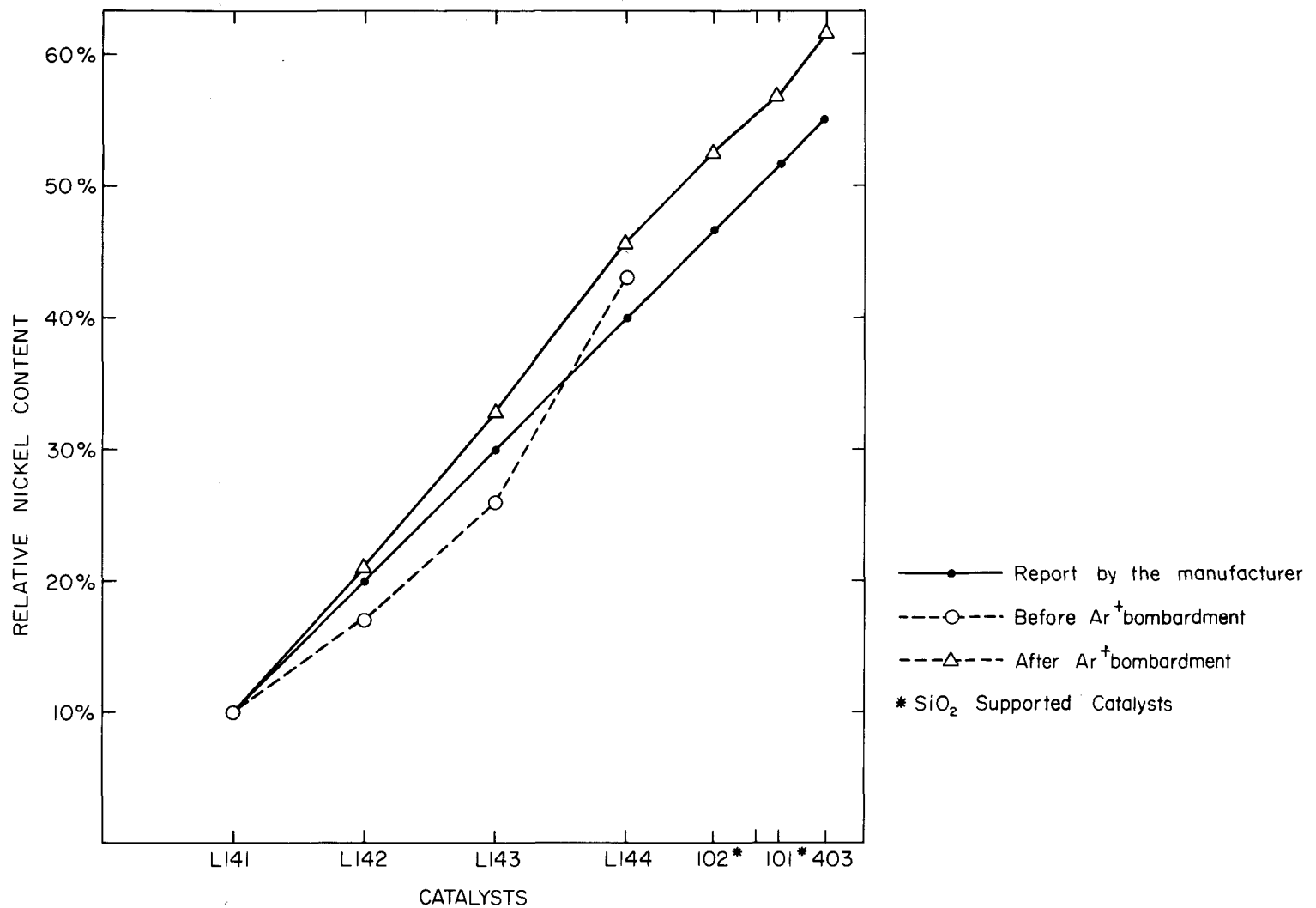

Figure IV C5. Ni content from relative Auger intensity as compared with stoichiometric Ni content.

(3) Prepare single crystal thin ribbon with (100) and (111) orientation.

(4) Install constant temperature controller.

(5) Investigate LEED change of Ni single crystal surface after adsorption of various amounts of SO_2 and H_2S.

(iii) References

(1) P. J. Reucroft, E. B. Bradley, R. J. De Angelis and G. A. Sargent. 1st Annual Report,"Surface Structure and Mechanisms of Gasification Catalyst Deactivation," February 1976 - January 1977, ERDA Contract No. E(49-18)2229.

(2) J. C. Tracy, Rev. Sci. Instr. 39, 1300 (1968).

(3) Catalysts and Chemicals, Inc., Louisville, Kentucky 40201.

(4) P. W. Palmberg, T. N. Rhodin, J. Appl. Phys. 392425 (1968).

(5) C. C. Chang, Surface Sci., 25 53 (1971).

D. REPORTING CATEGORY 4 - X-RAY DIFFRACTION CHARACTERIZATION OF CATALYST MATERIALS (Prepared by P. Ganesan and R. J. De Angelis)

(i) Work Accomplished

In the previous report,[1] the x-ray diffraction technique developed for determination of the particle size distribution function was successfully employed to characterize the as-received and sintered catalytic materials in the unreduced form. In order to apply this technique to the determination of the particle size distribution function of reduced nickel supported catalysts it is necessary to conduct reduction experiments to develop suitable procedures for sample preparation.

The reduction of NiO catalytic materials before the catalyst is put into service for methanation, is usually carried out at higher temperatures in comparison to the low temperature reduction that is possible with bulk nickel oxide. This is due to the fact that supported nickel oxide is much less reactive than when unsupported.[2] Also the degree of reduction of nickel in supported catalysts depends on the temperature of the calcination step prior to reduction,[3] method of preparation as to impregnation versus co-precipitation[4] and seldom reaches 100%. The degree of reduction generally increases with increasing reduction temperature[5]. However, high reduction temperature promotes extensive sintering of nickel. In order to reduce the sintering effect and maintain better activity it is therefore necessary to lower the reduction temperature as much as possible. To achieve this, it would be desirable to understand the reduction kinetics of NiO in these supported materials. During this reporting period, reduction kinetics data obtained on some of these catalytic materials are reported.

Reduction experiments were performed in hydrogen atmosphere using a Dupont Thermal Gravimetric Analyzer which automatically records the weight loss as a function of time at constant temperature. For each run approximately 10 mg of the sample taken from the as-received pellet is placed on the thermobalance. Initially the system is purged with dry nitrogen and the the apparatus is programmed for an isothermal run by setting the desired temperature. During initial heating there is weight loss due to removal of moisture and possibly adsorbed oxygen. Once a steady state is reached hydrogen is passed at a predetermined flow rate as measured by a flowmeter. The fractional reduction calculations are based on the sample weight after the moisture is removed. The fractional reduction R is given by:

$$R = W/W_0 \qquad (1)$$

where W is the weight loss and W_0 is the initial weight of oxygen. Initial weight of oxygen is calcualted assuming all nickel to be in the form of NiO.

Reduction experiments were carried out for C150-1-01 and C150-4-03 catalysts at 400, 450 and 500°C. Hydrogen flow rates of 4.8 and 8.0 cc/min were used for C150-1-01 and 4.8 cc/min for C150-4-03 catalyst. Times necessary to attain 50 and 70% reduction, along with sample weight and initial weight loss due to moisture for different flow rates and temperatures are recorded in Table 1. The fractional reduction with time obtained for C150-1-01 and C150-4-03 catalysts at different temperature and flow rates of hydrogen are plotted in Figure IV D1 and Figure IV D2 respectively.

In the case of silica supported C150-1-01 catalysts it is evident from Figure IV D1 that within five minutes almost 50% of NiO is reduced and the reaction rate is reduced considerably thereafter. Also the reaction does not

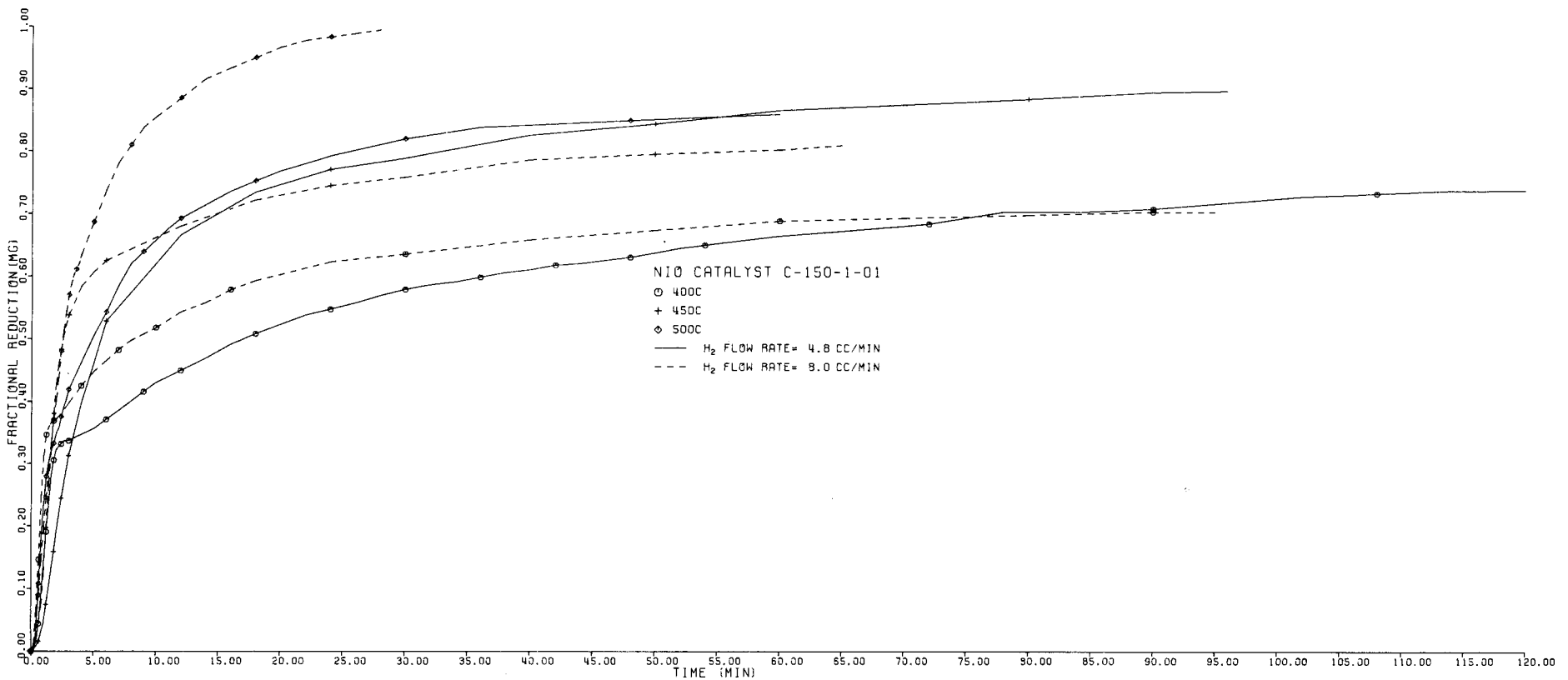

Figure IV D1. Reduction-time curves of silica supported C150-1-01 catalyst. Reduction temperatures and H_2 flow rates are as indicated.

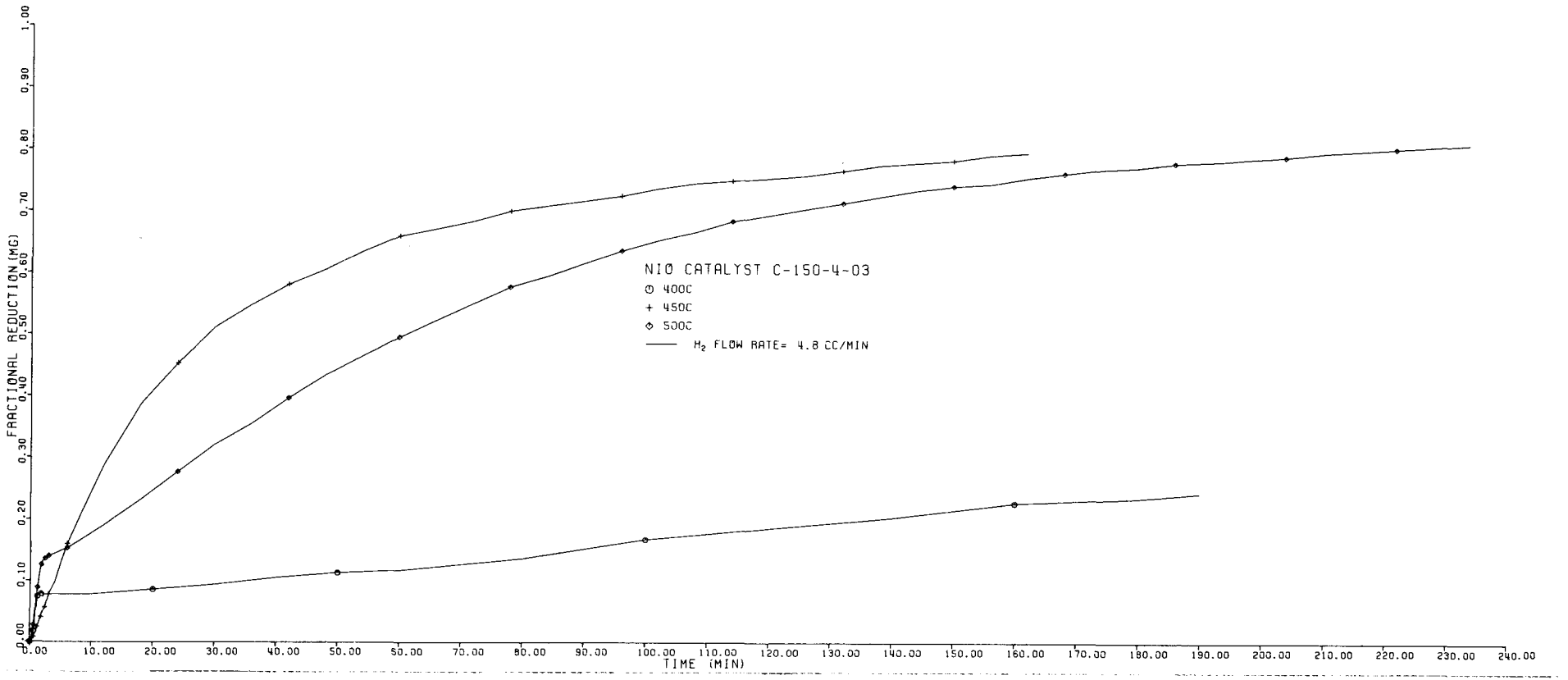

Figure IV D2. Reduction-time curves of alumina supported C150-4-03 catalyst at various temperatures.

go to completion in most of the cases. This indicates that there are probably two types of NiO that can be distinguished in these supported catalyst. Part of the nickel oxide that is readily accessible to hydrogen is reduced spontaneously and the other part corresponds to portions of NiO which are nearly completely encapsulated by the support. Thus the carrier has an inhibiting effect on the accessibility of hydrogen to this NiO thus effectively reducing the kinetics of reduction considerably in the later part of the reaction.

The influence of temperature on the reduction process is represented in Figures IV D3 - IV D6 for silica supported C150-1-01 catalysts. These are Arrhenius plots of the inverse t0.50 and t0.70 (times necessary to attain respectively 50 and 70% reduction) at hydrogen flow rates of 4.8 and 8.0 cc/min. The values of activation energy for 50 and 70% reduction at the hydrogen flow rate of 4.8 cc/min are respectively 13.4 and 19 Kcal/mole. The values are in very good agreement with the reported activation energies of 13.8 and 18.7 Kcal/mole for the permeability and diffusion of hydrogen in Nickel.[6] Thus it can be reasonably concluded that the permeability of hydrogen in the initial period and diffusion of hydrogen in the later part of the reduction process control the reaction kinetics. Effect of the supports is to limit the diffusion of hydrogen by impeding the accessibility of hydrogen to NiO thus reducing the kinetics of reduction. This is also consistent with the observation that almost 100% reduction could be attained within five minutes at 400°C in the case of pure NiO.

Increasing the flow rate of hydrogen increases the rate of reduction initially but has an adverse effect in the later part of the reduction process at reduction temperatures of 400 and 450°C. The reduction goes to near completion at 500°C with higher flow rates. The activation energies calculated from the Arrhenius plots shown in Figure IV D5 and IV D6 give values of 12.5 and 28.5

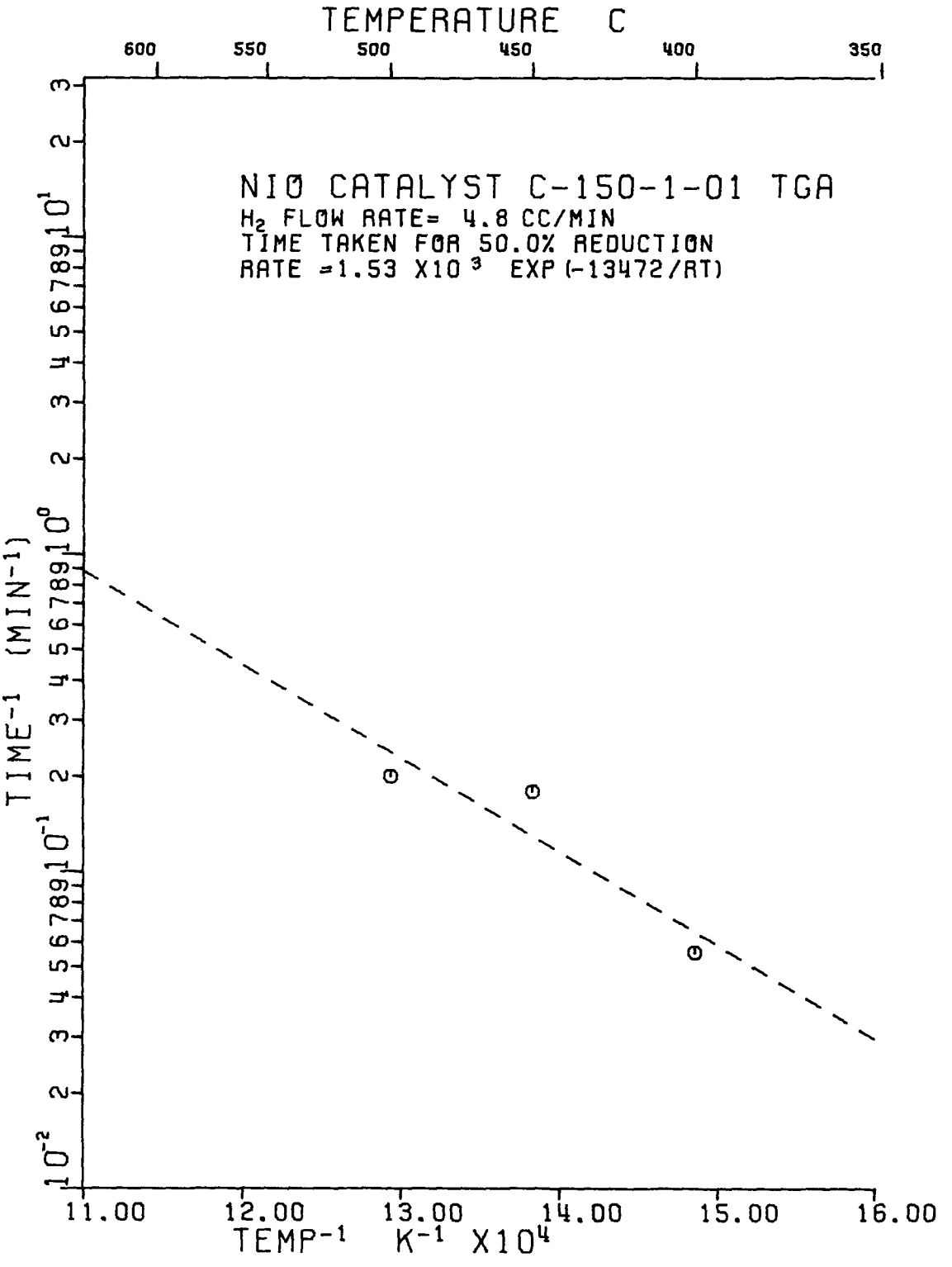

Figure IV D3. Effect of temperature on the time necessary for 50% reduction of C150-1-01 catalyst at a hydrogen flow rate of 4.8 cc/min.

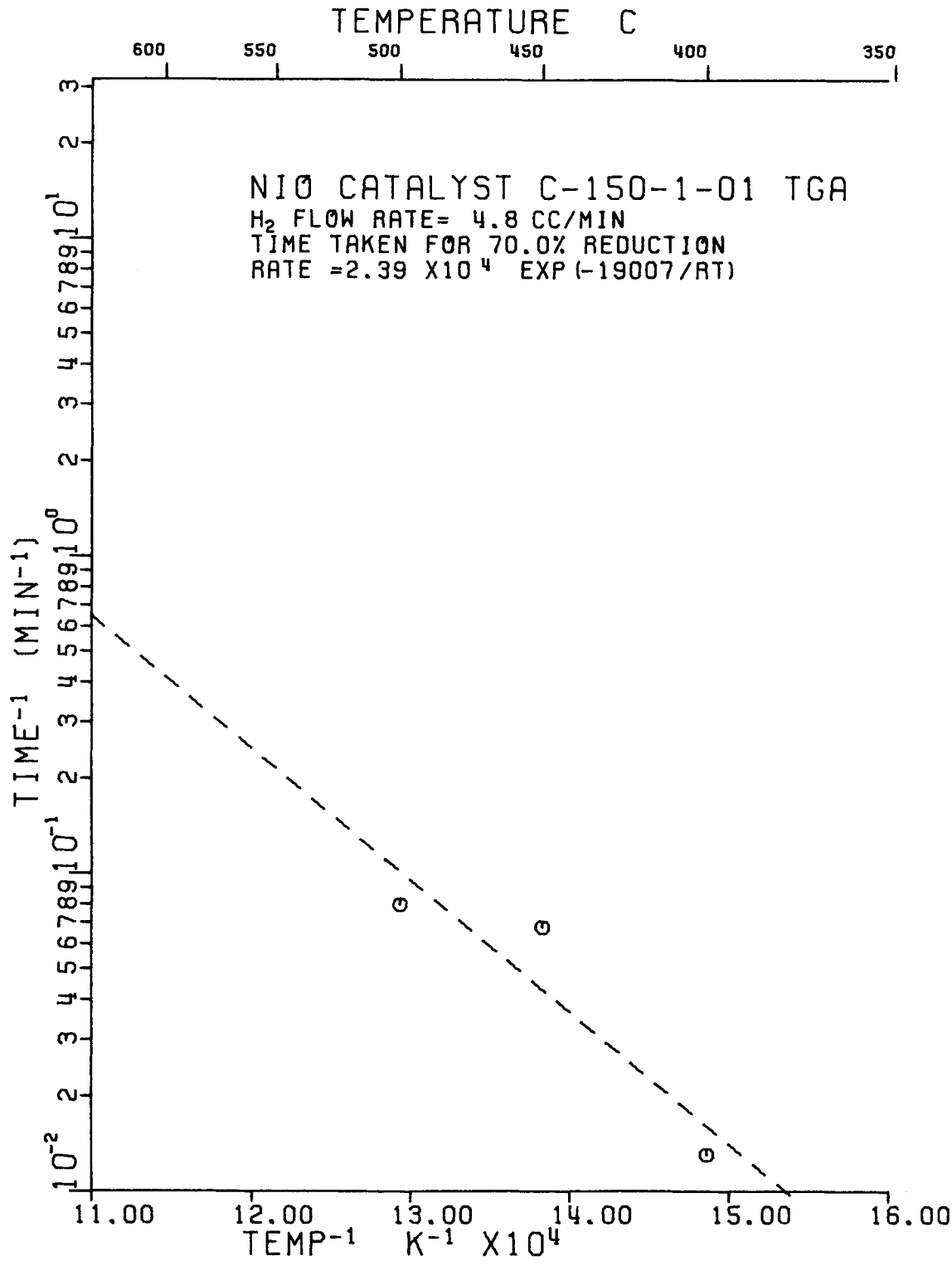

Figure IV D4. Effect of temperature on the time necessary for 70% reduction of C150-1-01 catalyst at a hydrogen flow rate of 4.8 cc/min.

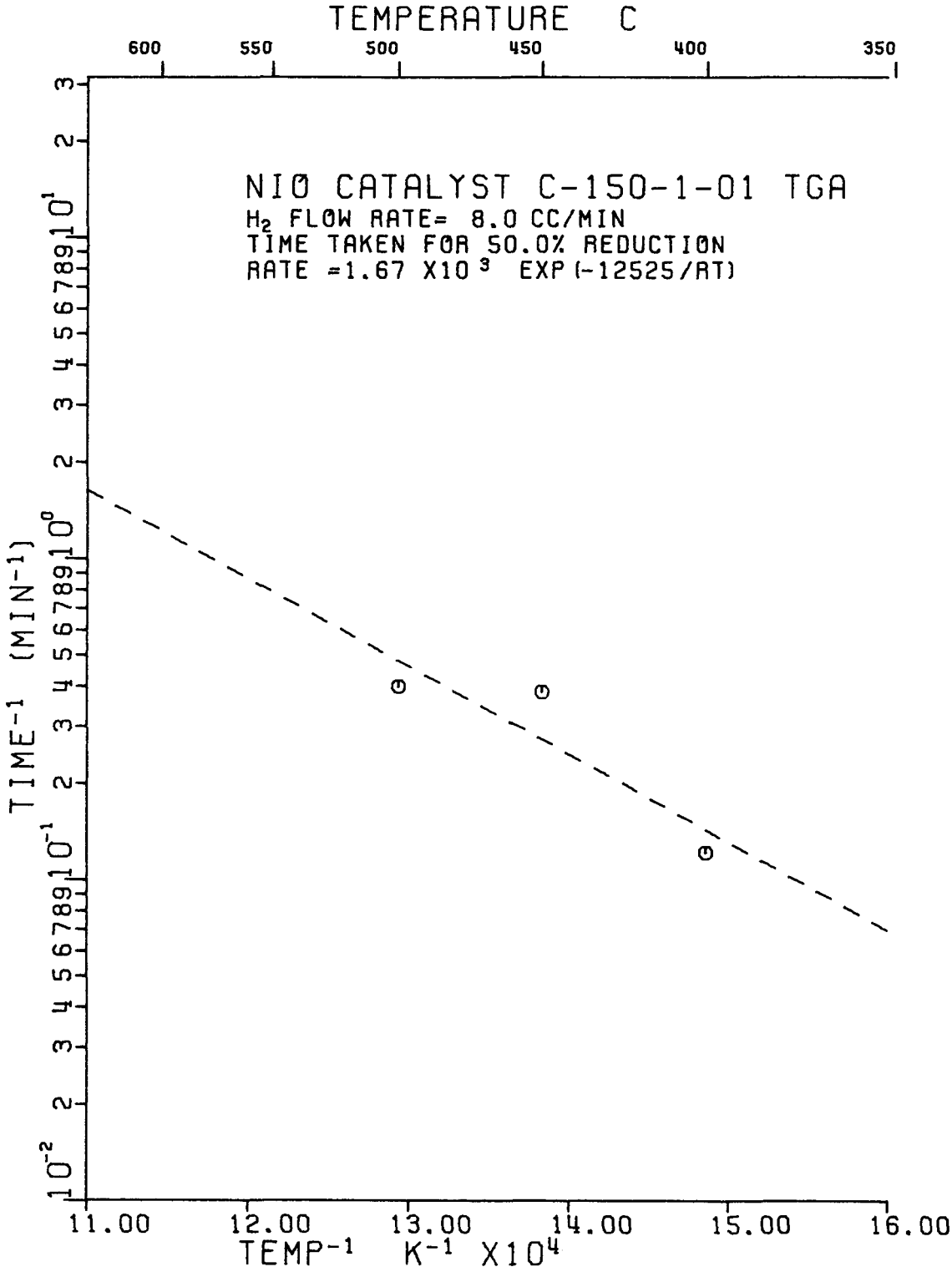

Figure IV D5. Effect of temperature on the time necessary for 50% reduction of C150-1-01 catalyst at a hydrogen flow rate of 8.0 cc/min.

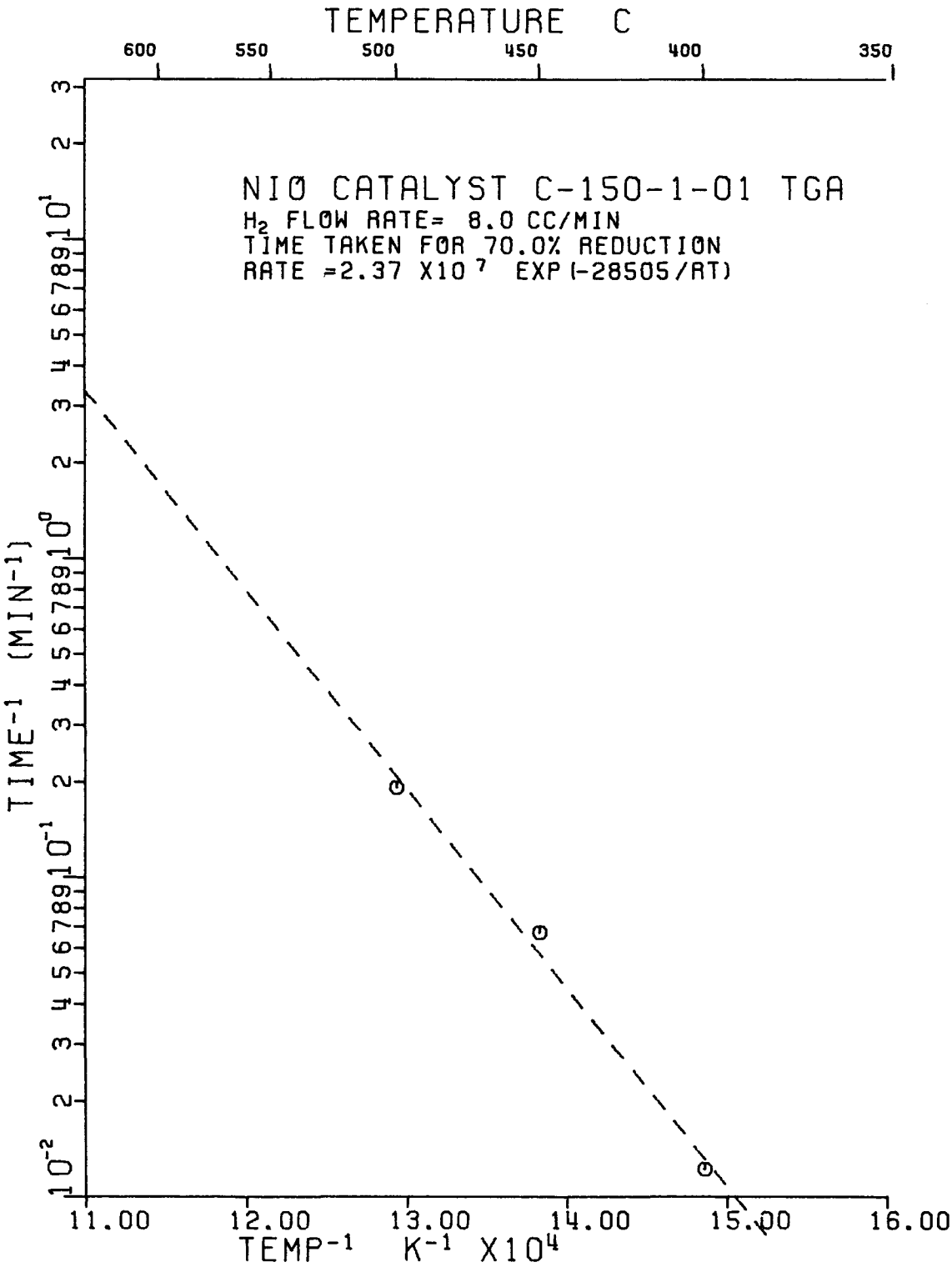

Figure IV D6. Effect of temperature on the time necessary for 70% reduction of C150-1-01 catalyst at a hydrogen flow rate of 8.0 cc/min.

Kcal/mole for 50 and 70% reduction at a hydrogen flow rate of 8.0 cc/min. At the present time the reason for lower kinetics at 400 and 450°C for higher hydrogen flow rate is not clear.

For the case of the alumina supported C150-4-03 catalyst, the data shown in Figure IV D2 indicates that the rate of reduction is slower than in the silica supported material. At a reduction temperature of 400°C, fractional reduction is only 25% and increases to 80% as the reduction temperature is increased. The data also indicates that the kinetics of reduction at 500°C is lower than at 450°C. This could be due to the combined effect of Al_2O_3 encapsulating NiO as well as possible reaction of NiO with alumina support to form nickel aluminate.

(ii) Work Forecast

In the next period reduction experiments by thermal gravimetric analysis will be continued further. X-ray diffraction work for the determination of the particle size distribution in reduced and passivated nickel supported catalysts will be resumed.

(iii) References

(1) P. J. Reucroft, E. B. Bradley, R. J. De Angelis and G. A. Sargent. First Annual Report, "Surface Structure and Mechanisms of Gasification Catalyst Deactivation," February 1, 1976 to January 31, 1977, ERDA Contract No. E(49-18)2229.

(2) A. Roman and B. Delmon, J. Catalysis, 30, 333 (1973).

(3) C. H. Bartholomew and R. J. Farrauto, J. Catalysis, 33, 41 (1976).

(4) V. C. F. Holm and A. Clark, J. Catalysis, 11, 305 (1968).

(5) G. A. Martin, N. Ceaphalan and P. Montogolfier, J. Chem. Phys., 70, 1422 (1973).

(6) W. Jost, "Diffusion in Solids, Liquids, Gases," Academic Press, New York (1960).

Table 1

Experimental data for reduction of different catalytic materials

Catalyst	Sample Wt. (mg)	Moisture Content (mg)	Reduction Temp. (°C)	H_2 Flow Rate (cc/min)	$^{\dagger}t_{0.5}$ (min)	$^{\dagger}t_{0.7}$ (min)
C150-1-01	9.10	1.54	400	4.8	18	76.8
C150-1-01	9.30	1.15	450	4.8	5.6	14.9
C150-1-01	8.42	1.54	500	4.8	5.0	12.6
C150-1-01	8.25	0.90	400	8.0	8.2	82.0
C150-1-01	9.05	1.01	450	8.0	2.6	15.0
C150-1-01	8.10	1.48	500	8.0	2.5	5.26
C150-4-03	9.40	0.66	400	4.8	--	--
C150-4-03	9.00	0.67	450	4.8	28.8	77.6
C150-4-03	10.92	0.88	500	4.8	60.9	123.0

† $t_{.50}$ and $t_{0.7}$ refers to time taken for 50 and 70% reduction resp.

V. CONCLUSIONS

1. NiS has a small degree of charging and small chemical shifts in comparison with the other standard samples examined. The ESCA spectrum appears to be very similar to that of nickel metal.

2. The average nickel (oxide) particle size in the unreduced L140 catalysts remains approximately equal to the electron mean free path (15-20Å). This is in agreement with previous results.

3. The charge corrected binding energies and singlet Ni 2p peak indicates that the surface of the L140 catalysts is composed of a nickel aluminate complex. The spectrum is unchanged after extended etching.

4. The exposure of a reduced C150-1-01 catalyst to a steam/synthesis gas flow under operating conditions leads to the formation of a nickel silicate or nickel hydroxide complex, particularly in the surface regions. NiO was not observed.

5. The reduction of an alumina based catalyst in a 1% H_2S/H_2 gas stream, which produces an inactive catalyst, has been observed to saturate the sample with sulfur (1:1 ratio of nickel to sulfur). Some sulfur is replaced by oxygen in the surface region of the sample. The exact form of the bonding cannot be specified, however.

6. Preliminary investigations on the kinetics of the reduction of silica and alumina supported nickel oxide indicate that, initially, part of the nickel oxide reduces spontaneously. At later stages there is a considerable drop in the rate of reduction.

7. The lower reduction rates observed during the later part of the reduction process may be due to portions of nickel oxide being completely encapsulated by the supports thus impeding the access of hydrogen to nickel-oxide.

8. Activation energies of 13 and 19 Kcal/mole (for 50 and 70% reduction) indicate that the permeability and diffusion of hydrogen are predominant rate controlling processes in the initial and later parts of the reduction, respectively.

9. The measurement of Auger intensity changes of Ni, Al and O after Ar^+ bombardment has indicated the presence of a contaminated layer about 400Å in depth.

10. The enhancement of the Ni Auger intensity is always greater than that of Al after Ar^+ bombardment. Thus, NiO particles are more susceptible to the contamination than Al_2O_3 particles.

11. The intensity of the Ni Auger peak is proportional to the stoichiometric Ni content of the catalysts and is independent of the support material (SiO_2 or Al_2O_3). This leads to the conclusion that the Auger escape depth for these two different types of catalysts is about the same. The Auger intensity could thus be employed for quantitative analysis of both types of catalysts without any need of complicated calibration.

12. The Raman bands of SiO_2 and Al_2O_3 are very weak and hence should not mask bands which are associated with adsorbed gases.

13. (2) Current investigations indicate that the fluorescence background will not hinder Raman spectra acquisition of the silica or alumina support catalysts.

14. (3) The alumina-support catalyst which had been pre-sulphided (ERDA Test 3) shows sulphate and/or sulphite bands in its Raman spectrum.

☆ U.S. GOVERNMENT PRINTING OFFICE: 1978-740-094/1096